Macromolecules
ARTICLE

*Macromolecules* **2010**, *43*, 6685–6698 **6685**
DOI: 10.1021/ma101088f

# Tuning the Optoelectronic Properties of Vinylene-Linked Donor−Acceptor Copolymers for Organic Photovoltaics

**Sangwon Ko,[†] Rajib Mondal,[‡] Chad Risko,[§] Jung Kyu Lee,[†] Sanghyun Hong,[‡] Michael D. McGehee,[⊥] Jean-Luc Brédas,[§] and Zhenan Bao*,[‡]**

[†]*Department of Chemistry, Stanford University, Stanford, California 94305,* [‡]*Department of Chemical Engineering, Stanford University, Stanford, California 94305,* [§]*School of Chemistry and Biochemistry, Georgia Institute of Technology, Atlanta, Georgia 30332, and* [⊥]*Department of Materials Science and Engineering, Stanford University, Stanford, California 94305*

*Received May 16, 2010; Revised Manuscript Received June 28, 2010*

ABSTRACT: Five new donor−acceptor copolymers containing the electron acceptor benzothiadiazole (**BTZ**) linked to the electron donors fluorene (**FL**) or cyclopentadithiophene (**CPDT**) via vinylene units were synthesized to study polymer structure−property relationships in organic photovoltaic devices. Both alternating (**P**) and random copolymers (**P1**−**P4**) were prepared via Suzuki and Stille polycondensations, respectively. The cyclopentadithiophene copolymers (**P2** and **P4**) have smaller electrochemical band gaps (1.79 and 1.64 eV) compared to the fluorene-containing copolymers (2.08 and 1.95 eV for **P1** and **P3**). However, the presence of **CPDT** raises the electrochemical HOMO energy levels (−4.83 and −4.91 eV for **P2** and **P4**) compared to the **FL** copolymers (−5.06 and −5.15 eV for **P1** and **P3**) leading to small open circuit voltages ($V_{oc}$) in solar cells. The primary solution and thin-film UV−vis absorption peaks of **P3** and **P4**, which do not contain alkylated thiophenes appended to the **BTZ** unit, are at lower energy and have larger absorption coefficients than their **P1** and **P2** counterparts. Detailed theoretical analyses of the geometric structure, electronic structure, and excited-state vertical transitions using density functional theory provide direct insight into the interplay between the structural modifications and resulting electronic and optical changes. A high molecular weight ($M_n$ = 25 kg/mol) polymer with a large degree of polymerization ($DP_n$ = 21) was easily achieved for the random copolymer **P1**, leading to thin films with both a larger absorption coefficient and a larger hole mobility compared to the analogous alternating polymer **P** ($M_n$ = 22 kg/mol, $DP_n$ = 18). An improved short circuit current and a power conversion efficiency up to 1.42% ($J_{sc}$ = 5.82 mA/cm$^2$, $V_{oc}$ = 0.765 V, and FF = 0.32) were achieved in bulk heterojunction solar cells based on **P1**.

## Introduction

The development of efficient organic photovoltaics (OPVs), specifically bulk heterojunction (BHJ) polymer-based solar cells, has become an active area of research in recent years due to their potential as alternative, clean energy sources.[1] Polymer BHJ solar cells offer the advantages of low-cost, large-scale fabrication by solution processing techniques, and compatibility with flexible and lightweight plastic substrates.[2] Poly(3-hexylthiophene) (**P3HT**) is one of the most commonly studied donor materials, with a power conversion efficiency (PCE) of about 5% achieved for BHJ solar cells based on **P3HT** and [6,6]-phenyl $C_{61}$-butyric acid methyl ester ($PC_{61}BM$).[3] However, it is difficult to further improve the efficiency of **P3HT**-based solar cells due to a limited low-energy absorption (optical band gap ∼2 eV) and a small energy offset between the HOMO of **P3HT** and LUMO of $PC_{61}BM$.

For a polymer to serve as an effective donor material in BHJ solar cells, a number of properties are considered necessary, including: broad absorption from the solar spectrum for efficient light harvesting; efficient charge transfer to the acceptor material (typically fullerene derivatives); effective charge transport; relatively deep HOMO energies to yield a large short circuit current ($J_{sc}$), fill factor (FF), and open circuit voltage ($V_{oc}$).[1c] Frontier molecular orbital energies and optical band gaps of donor polymers have been tuned through the use of a variety of backbones and side chains in order to enhance OPV efficiency.[4] In particular, the combination of electron-rich and electron-poor moieties has been successfully used to achieve low optical band gap polymers with suitable electronic energy levels. Benzothiadiazole (**BTZ**),[5] quinoxaline (**QX**),[6] and thienopyrazine (**TP**)[7] are commonly used acceptor units, while cyclopentadithiophene (**CPDT**),[5b−e,j] fluorene (**FL**),[6,7a−7c] and carbazole (**CZ**)[4a,5a,5h] are among the more commonly used donor units. Specifically, polymers containing **BTZ** and various donor units, such as **CPDT** and dithienosilole,[5f] have been shown to be very successful in BHJ solar cells with PCEs of greater than 5%.

In addition to frontier molecular orbital energy and optical band gap engineering, developing polymers with large absorption coefficients is important so as to maximize the solar cell photocurrent;[1c] generally, the amount of absorbed light depends both on the absorption wavelength and on the intensity of the absorption. Recently, we reported **ACT-FL** polymers with enhanced solar cell efficiency by increasing the optical absorption.[7a] Removing the imposed twists increased the HOMO−LUMO overlap and enhanced the absorption coefficient for the lowest optical transition ($S_0 \rightarrow S_1$), which is typically dominated by a charge-transfer (HOMO → LUMO) electronic excitation.

Incorporating vinylene groups in $\pi$-conjugated systems is a further strategy that can be effective for tuning electronic and optical properties.[8] The vinylene linkage serves to planarize the polymer backbone and extend the $\pi$-conjugation by further

*Corresponding author. E-mail: zbao@stanford.edu.



Published on Web 07/20/2010

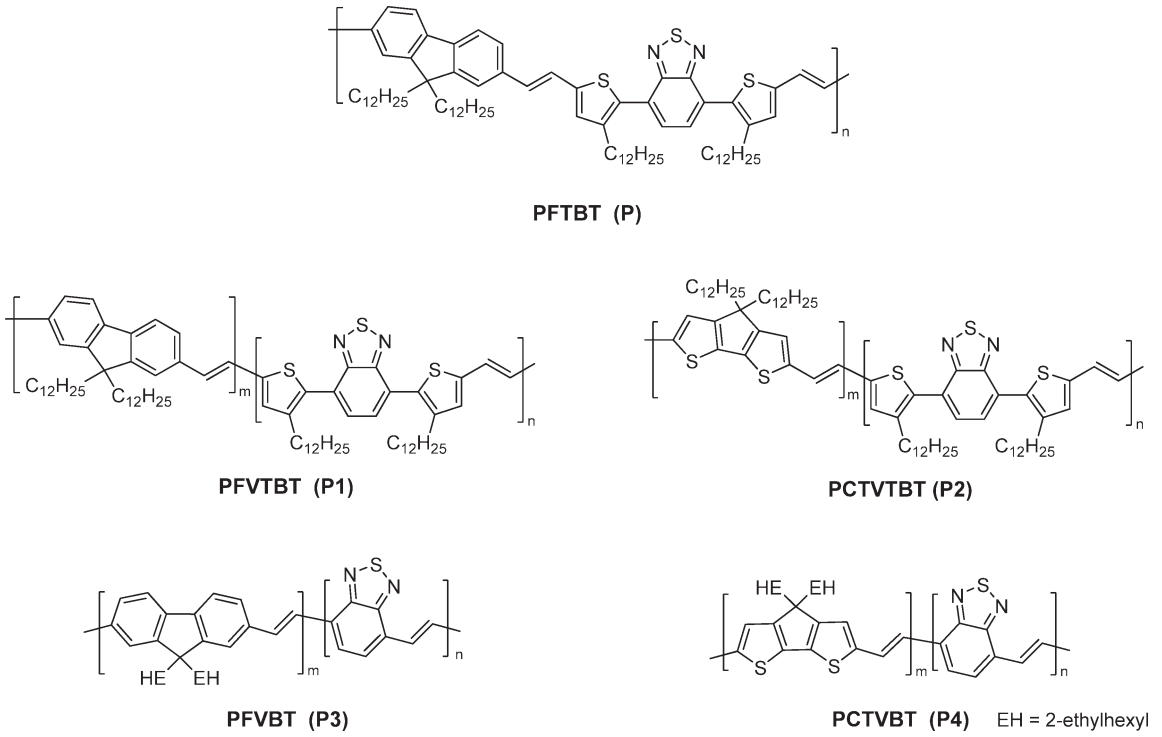


**Figure 1.** Structures of the vinylene-linked alternating polymer **PFVTBT** (**P**) and random polymers **PFVTBT** (**P1**), **PCTVTBT** (**P2**), **PFVBT** (**P3**), and **PCTVBT** (**P4**), *m*:*n* = 1:1 for **P1**−**P4** polymers.

eliminating torsional strains between the donor and acceptor units, leading to a lower optical band gap and a more broadly absorbing material.[9] For example, poly(3-hexyl thienylenevinylene) (**P3HTV**)[8a] and a vinylene-linked benzothiadiazole-thiophene (**PTVBT**)[8b] show broader absorptions with lower band gaps compared to their analogous polymers with thiophene linkages. 2,7-carbazole-based vinylene-incorporating copolymers[8c] have also been reported for solar cell applications; unfortunately, solar cell efficiencies with these materials were poor (0.2−0.8%), with the low performance attributed to an extremely short singlet excited-state lifetime,[8a] low molecular weight ($M_n$ = 2.8−4.3 kg/mol),[8c] and coarse phase separation of the polymer:PCBM blend.[8b] The PCEs of the recently reported vinylene-linked 4,7-diphenyl-2,1,3-benzothiadiazole-based polymers (poly(fluorenevinylene-*alt*-4,7-diphenyl-2,1,3-benzothiadiazole, **PF-DBT**, and poly(phenylenevinylene-*alt*-4,7-diphenyl-2,1,3-benzothiadiazole, **PP-DBT**) have improved to 1.25 and 1.62%, respectively.[8d] **PF-DBT** and **PP-DBT** copolymers exhibit high molecular weights ($M_n$ = 29 and 62 kg/mol, respectively), stable HOMO levels (−5.45 and −5.23 eV, respectively), and uniform films for polymer:PCBM blends. However, they have relatively narrow absorption ranges and large band gaps ($\lambda_{onset}$ = ∼534 and 554 nm, $E_g^{opt}$ = 2.32 and 2.24 eV, respectively), which limit the photocurrent generation ($J_{sc}$ = 2.80 and 3.93 mA/cm$^2$, respectively).

In this work, five new donor−acceptor copolymers containing the electron acceptor benzothiadiazole (**BTZ**) linked to the electron donors fluorene (**FL**) or cyclopentadithiophene (**CPDT**) via vinylene or vinylene−alkylated-thienylene units were designed and synthesized for use in BHJ solar cell applications (Figure 1). **BTZ** effectively lowers the polymer LUMO energy while keeping the HOMO energy almost constant, leading to near optimum energy levels for photovoltaic applications.[10] Though the alkylated-thiophene units induce steric twists in the conjugated backbone, they could provide for more coplanar structures and extended π-conjugation compared to the phenylene linkages in **PF-DBT** and **PP-DBT**.[11] Alternating (**P**) and random (**P1**) **FL**-based copolymers were investigated to compare the effects of molecular weight and absorption coefficients on the photovoltaic properties. To prepare the vinylene-containing donor−acceptor copolymers (i.e., **PF-DBT** and **PP-DBT**), the Horner−Emmons coupling reaction between dialdehyde and diphosphonate derivatives is commonly used, owing to its strict regioselectivity.[8c,d] Our polymers were synthesized by using Suzuki and Stille polycondensations due to the facile preparation of monomers and the greater functional group compatibility of these reaction conditions.[8b] For direct comparison of the opto-electronic properties, **P3**, which does not contain the alkylated-thiophene groups around **BTZ**, was synthesized. **CPDT**-based polymers (**P2** and **P4**) were synthesized for further comparison as lower band gaps were expected. Cyclic voltammetry, optical absorption, and theoretical calculations using density functional theory were employed to characterize the structure−property relationships of the five new polymer systems. Hole mobilities and solar cell performance were also measured as a test of the employed polymer design principles.

## Experimental Section

**Materials.** 4*H*-Cyclopenta[2,1-*b*:3,4-*b*′]dithiophene,[12] 2,6-dibromo-4,4-diethylhexyl-4*H*-cyclopenta[2,1-*b*:3,4-*b*′]dithiophene (**7**),[12] 2-(3-dodecyl-2-thienyl)-4,4,5,5-tetramethyl-1,3,2-dioxaborolanes,[13] and 4,7-dibromo-2,1,3-benzothiadiazole (**8**)[14] were prepared according to the reported procedures. *N*,*N*-Dimethylformamide (DMF) and toluene were purified through the Pure Sol-MD Standard Design Solvent Purification System, Innovative Technology Inc. *trans*-1,2-Bis(tributylstannyl)ethylene (**4**), tributyl(vinyl)-tin, 9,9-di(2′-ethylhexyl)-2,7-dibromofluorene (**6**), tris[dibenzylideneacetone]dipalladium(0), tetrakis(triphenylphosphine)palladium (0), Aliquat336, chlorobenzene, dimethyl sulfoxide (DMSO), potassium iodide, and potassium hydroxide (KOH) were purchased from Aldrich, Strem, TCI America, or Alfa Aesar and used without further purification. *N*-Bromosuccinimide (NBS) and 9,9-didodecyl-2,7-dibromofluorene (**3**) were purchased from Aldrich and used after recrystallization from distilled water and hexane, respectively.

**Measurements and Characterization.** $^1$H and $^{13}$C NMR spectra were recorded using Varian Inova 300, Merc 400, or Inova 500 in $CDCl_3$ at 293 K. Gel permeation chromatography (GPC) was performed in THF. Molecular weights were determined by size exclusion chromatography with Viscotec GPC system (Model 350 HTGPC) in THF. The calibration curve was made with monodipersed polystyrene standards. Thermal gravimetric analyses (TGA) were carried out using a Mettler TOLEDO TGA/SDTA 851e at a heating rate of 10 °C/min under a nitrogen flow of 20 mL/min. Differential scanning calorimetry (DSC) analyses were performed on a DSC Q100 (TA Instruments). DSC curves were recorded at a scanning rate of 10 °C min under a nitrogen flow.

Electrochemical analyses were carried out by cyclic voltammetry using a CHI411 instrument from CH Instruments, Inc. The experiments were performed under a stream of argon in a saturated solution of 0.05 M tetra-*n*-butylammonium hexafluorophosphate ($n$-$Bu_4NPF_6$, from Strem Chemicals, Inc., recrystallized from ethanol) as a supporting electrolyte in anhydrous 1,2-dichlorobenzene (ODCB). The experiments were carried out using platinum electrodes at a scan rate of 100 mV $s^{-1}$ against Ag wire as a pseudoreference electrode at ambient temperature. The $Fc/Fc^+$ redox couple was used as a reference oxidation potential for the electrochemical measurements.

UV−vis−NIR absorption spectra were recorded in a UV−vis spectrophotometer (Cary 6000i) at room temperature using a quartz cuvette with a path length of 1 cm. Thin films for solid-state UV−vis were prepared by drop casting on glass from polymer solutions in ODCB. Optical band gaps were calculated from the onset of the longest wavelength absorption bands of the thin film. Thickness measurements were performed with a Dektak 150 profilometer (Veeco Metrology Group).

Hole mobilities were evaluated with a diode configuration of ITO/PEDOT:PSS/polymer/Au by taking the current−voltage current in the range of 0−5 V and using the space charge limited current (SCLC) model (eq 1),

$$J = 9\varepsilon_0\varepsilon_r\mu V^2/8L^3 \quad (1)$$

where is $\varepsilon_0$ is the permittivity of free space, $\varepsilon_r$ is the dielectric constant of the polymer, $\mu$ is the hole mobility, $V$ is the voltage drop across the device, and $L$ is the polymer thickness.[15]

Tapping mode AFM investigations of the polymer films were carried out using a Multimode Nanoscope III with Extender electronics (Digital Instruments/Veeco Metrology Group).

**Synthesis.** *2,7-Bis(4′,4′,5′,5′,-tetramethyl-2′-vinyl-1′,3′,2′-dioxaborate)-9,9-bis(2-dedecyl)fluorene* (***1***). Triethyl amine (3.1 g, 30 mmol) was added to the mixture of 9,9-didodecyl-2,7-dibromofluorene (2.0 g, 3.0 mmol), 4,4,5,5,-tetramethyl-2-vinyl-1,3,2-dioxaborolane (956 mg, 6.2 mmol), palladium acetate (34 mg, 0.15 mmol), and tri-*o*-tolylphosphine (184 mg, 0.2 mmol) in 40 mL of anhydrous DMF under argon. After heating at 110 °C for 7 h, the reaction mixture was washed with brine solution several times and the organic layer was extracted with ethyl acetate. The organic layer was dried over $MgSO_4$ and the filtrate was concentrated to be subjected to silica gel column chromatography eluting with hexane/dichloromethane (5:1) followed by hexane/ethyl acetate (5:1) to afford pure compound **1** as a yellowish oil (167 mg, 69%). $^1$H NMR (300 MHz, $CDCl_3$): $\delta$ 0.58 (m, 4H), 0.86 (t, $J$ = 6.6 Hz, 6H), 1.01−1.32 (m, 60H), 1.92 (m, 4H), 6.22 (d, $J$ = 18.6 Hz, 2H), 7.45 (s, 4H), 7.50 (d, $J$ = 19.2 Hz, 2H), 7.63 (m, $J$ = 8.1 Hz, 2H). $^{13}$C NMR (75 MHz, $CDCl_3$): $\delta$ 14.20, 22.76, 23.86, 24.90, 29.35, 29.39, 29.61, 29.67, 30.14, 31.97, 40.47, 54.90, 83.39, 120.04, 121.57, 126.34, 136.66, 141.73, 150.11, 151.67. HRMS (ESI): $m/z$ = 829.6467 ($M + Na^+$); calcd $m/z$ = 829.6477.

*4,7-Bis(3-dodecyl-2-thienyl)-2,1,3-benzothiadiazole*. 4,7-Dibromo-2,1,3-benzothiadiazole (0.92 g, 3.13 mmol), 2-(3-dodecyl-2-thienyl)-4,4,5,5-tetramethyl-1,3,2-dioxaborolane (2.5 g, 6.60 mmol), tetrakis(triphenylphosphine)palladium (0) (0.185 g, 0.16 mmol, 8.1 mol %), and Aliquat336 (0.64 g, 1.58 mmol) were dissolved in 40 mL of toluene and stirred for 10 min under argon. 2 M aqueous solution of degassed aq. $K_2CO_3$ (16 mL) was added and the reaction mixture was stirred at 90−95 °C for 24 h. After removal of the solvent using a rotary evaporator, the residue was extracted with dichloromethane and washed with brine solution. The organic layer was dried over $MgSO_4$. The crude product was subjected to silica gel column chromatography eluting with hexane/ethyl acetate (5:1) to afford 4,7-bis(3-dodecyl-2-thienyl)-2,1,3-benzothiadiazole (1.32 g, 66%). $^1$H NMR (500 MHz, $CDCl_3$): $\delta$ 0.87 (t, $J$ = 7.5 Hz, 6H), 1.18−1.29 (m, 36H), 1.59−1.65 (m, 4H), 2.66 (t, $J$ = 8.0 Hz, 4H), 7.10 (d, $J$ = 8.5 Hz, 2H), 7.44 (d, $J$ = 9.0 Hz, 2H), 7.64 (s, 2H). $^{13}$C NMR (125 MHz, $CDCl_3$): $\delta$ 14.22, 22.77, 29.44, 29.48, 29.54, 29.63, 29.71, 29.75, 30.81, 32.00, 125.95, 127.51, 129.31, 129.98, 132.23, 141.79, 154.36. HRMS (ESI): $m/z$ = 637.3690 ($M + H^+$); calcd $m/z$ = 637.3678.

*4,7-Bis(5-bromo-3-dodecyl-2-thienyl)-2,1,3-benzothiadiazole* (***2***). To a mixture of 4,7-bis(3-dodecyl-2-thienyl)-2,1,3-benzothiadiazole (1.32 g, 2.07 mmol) in 10 mL of DMF was added *N*-bromosuccinimide (0.81 g, 4.55 mmol) at room temperature under an argon atmosphere. The resulting mixture was stirred for 4 h. The reaction mixture was diluted with chloroform and washed with water several times. The organic extraction was dried with $MgSO_4$ and evaporation in vacuo. The residue was purified by column chromatography on silica gel with hexane/ethyl acetate (5:1) as the eluent, yielding compound **2** as a yellow solid (yield = 1.46 g, 89%). $^1$H NMR (400 MHz, $CDCl_3$) $\delta$ 0.87 (t, $J$ = 7.2 Hz, 6H), 1.19−1.29 (m, 36H), 1.58−1.62 (m, 4H), 2.61 (t, $J$ = 8.0 Hz, 4H), 7.06 (s, 2H), 7.60 (s, 2H); $^{13}$C NMR (100 MHz, $CDCl_3$) $\delta$ 14.22, 22.77, 29.42, 29.47, 29.59, 29.70, 29.71, 29.74, 30.61, 32.00, 113.28, 126.66, 129.77, 132.06, 133.60, 142.51, 153.99; HRMS (ESI) $m/z$ = 793.1873 ($M + H^+$), calcd $m/z$ = 793.1889.

*4,4-Didodecyl-4H-cyclopenta[2,1-b:3,4-b′]dithiophene*. To a solution of 4*H*-cyclopenta[2,1-*b*:3,4-*b*′]dithiophene (0.96 g, 5.4 mmol) in 25 mL of DMSO, 1-bromododecane (2.7 g, 10.8 mmol), a catalytic amount of potassium iodide (25 mg), and finely ground KOH (0.96 g, 17 mmol) were added under argon. The resulting solution was vigorously stirred at room temperature overnight. The reaction mixture was cooled to 0 °C and 25 mL of water was added. The product was extracted in ether, followed by washing with brine solution. The ether layer was dried with $MgSO_4$ and evaporation in vacuo. The residue was purified by column chromatography on silica gel with hexane as the eluent, yielding 4,4-didodecyl-4*H*-cyclopenta[2,1-*b*:3,4-*b*′]dithiophene as colorless liquid (yield = 2.51 g, 91%). $^1$H NMR (400 MHz, $CDCl_3$): $\delta$ 0.80−1.00 (m, 10H), 1.10−1.30 (m, 36H), 1.83 (m, 4H), 6.93 (d, $J$ = 4.8 Hz, 2H), 7.14 (d, $J$ = 4.8 Hz, 2H). $^{13}$C NMR (100 MHz, $CDCl_3$): $\delta$ 14.38, 22.94, 24.77, 29.59, 29.65, 29.84, 29.88, 30.28, 32.16, 37.96, 53.47, 121.88, 124.63, 136.65, 158.37. HRMS (ESI): $m/z$ = 515.3747 ($M + H^+$); calcd $m/z$ = 515.3740.

*2,6-Dibromo-4,4-didodecyl-4H-cyclopenta[2,1-b:3,4-b′]dithiophene* (***5***). NBS (0.464 g, 2.56 mmol) in 10 mL of DMF was added dropwise to a solution of 4,4-didodecyl-4*H*-cyclopenta-[2,1-*b*:3,4-*b*′]dithiophene (0.66 g, 1.28 mmol) in 15 mL of DMF at room temperature for 30 min under argon. The reaction mixture was stirred overnight. The resulting solution was poured into water and extracted with $CH_2Cl_2$. The crude product was then subjected to silica column chromatography with hexane to afford compound **5** (yield = 0.50 g, 59%). $^1$H NMR (400 MHz, $CDCl_3$): $\delta$ 0.86−0.92 (m, 10H), 1.14−1.30 (m, 36H), 1.73−1.78 (m, 4H), 6.93 (s, 2H). $^{13}$C NMR (100 MHz, $CDCl_3$): $\delta$ 14.23, 22.79, 24.52, 29.44, 29.69, 29.73, 30.03, 32.01, 37.61, 55.09, 111.16, 124.65, 136.36, 156.00; HRMS (ESI): $m/z$ = 671.1945 ($M + H^+$); calcd $m/z$ = 671.1950.

*Poly[9,9-didodecyl-2,7-fluoreneylenevinylene-alt-4′,7′-bis(3-dodecyl-2-thienyl)-2′,1′,3′-benzothiadiazole]* (*alternating-**PFVTBT***, ***P***). Potassium carbonate solution (2 M in water, 0.8 mL) was added to a mixture of compound **1** (161 mg, 0.20 mmol),

compound **2** (159 mg, 0.20 mmol), tetrakis(triphenylphosphine)palladium (0) (6.9 mg, 0.006 mmol), and Aliquat336 (40 mg) in 2.5 mL of toluene under argon. The reaction mixture was frozen and degassed under vacuum three times. Then the reaction mixture was heated to 90−95 °C and stirred for 3 days. The polymer was end-capped with a phenyl group by an adding excess of phenylboronic acid and bromobenzene. Crude polymers were precipitated in methanol and washed with hexane and acetone. The polymer was redissolved in 10 mL of chloroform along with Pd(0) scavenger[16] and stirred at room temperature overnight. The polymer was collected by reprecipitation and filtration from methanol. After washing the final product using Soxhlet apparatus with methanol, acetone, and hexane, the polymer **P** was obtained as a red solid (161 mg, 68%). GPC: $M_n$ = 22 kg/mol, $M_w$ = 81 kg/mol, PDI = 3.67. $^1$H NMR (500 MHz, $CDCl_3$): $\delta$ 0.67 (br, 4H), 0.84−0.87 (m, 12H), 1.08−1.23 (br, 72H), 1.68 (br, 4H), 2.01 (br, 4H), 2.68 (br, 4H), 7.08−7.13 (br, 4H), 7.29−7.32 (br, 2H), 7.44−7.47 (br, 4H), 7.68 (br, 4H). Anal. Calcd for $C_{79}H_{114}N_2S_3$: C, 79.87; H, 9.67; N, 2.63; S, 8.10. Found: C, 77.56; H, 9.53; N, 2.44; S, 7.58.

*Poly*[*9,9-didodecyl-2,7-fluoreneylenevinylene-alt-4′,7′-bis*(*3-dodecyl-2-thienyl*)*-2′,1′,3′-benzothiadiazole*] (*random-**PFVTBT**, **P1***). Tris[dibenzylideneacetone]dipalladium(0) (9.16 mg, 0.005 mmol) was added to a mixture of 9,9-didodecyl-2,7-dibromofluorene (132 mg, 0.20 mmol, *trans*-1,2-bis(tributylstannyl)ethylene and compound **3** (159 mg, 0.20 mmol), (3,3′-didodecyl-2,2′-bithiophene-5,5′-diyl)bis(trimethylstannane) (242 mg, 0.40 mmol), and tri(*o*-tolyl)phosphine (18.3 mg, 0.06 mmol) in 4 mL of chlorobenzene under argon. The reaction mixture was frozen and degassed under vacuum three times. The reaction mixture was heated to 95−100 °C and stirred for 3 days. The raw product was precipitated in methanol and collected by filtration. The crude polymer was purified according to the same procedure as **P**. Yield = 58% (138 mg). GPC: $M_n$ = 25 kg/mol, $M_w$ = 40 kg/mol, PDI = 1.60. $^1$H NMR (500 MHz, $CDCl_3$): $\delta$ 0.67 (br, 4H), 0.84−0.87 (m, 12H), 1.08−1.25 (br, 72H), 1.67 (br, 4H), 2.02 (br, 4H), 2.68 (br, 4H), 7.08−7.13 (br, 4H), 7.29−7.33 (br, 2H), 7.45−7.52 (br, 4H), 7.69 (br, 4H). Anal. Calcd for $C_{79}H_{114}N_2S_3$: C, 79.87; H, 9.67; N, 2.63; S, 8.10. Found: C, 75.93; H, 9.28; N, 2.61; S, 8.14.

*Poly*[*2,6-*(*4,4-didodecyl*)*-4H-cyclopenta*[*2,1-b:3,4-b′*]*dithiopheneylenevinylene*)*-alt-4,7-bis*(*3-dodecyl-2-thienyl*)*-2,1,3-benzothiadiazole*] (***PCPDTVTBT**, **P2***). The polymer was synthesized following the same procedure as **P1** with the respective monomers. Yield = 79%. GPC: $M_n$ = 13 kg/mol, $M_w$ = 22 kg/mol, PDI = 1.68. $^1$H NMR (500 MHz, $CDCl_3$): $\delta$ 0.89 (br, 4H), 0.99 (br, 4H), 1.23−1.17 (br, 72H), 1.66 (br, 4H), 1.81 (br, 4H), 2.67 (br, 48H), 7.12−6.86 (br, 8H), 7.68 (br, 2H). Anal. Calcd for $C_{75}H_{110}N_2S_5$: C, 75.07; H, 9.24; N, 2.33; S, 13.36. Found: C, 73.42; H, 9.19; N, 2.29; S, 12.84.

*Poly*[*9,9-bis*(*2-ethylhexyl*)*-2,7-fluoreneylenevinylene-alt-4,7-*(*2,1,3-benzothiadiazole*)] (***PFVBT**, **P3***). The polymer was synthesized following the same procedure as **P1** with respective the monomers. Yield = 67%. GPC: $M_n$ = 8.1 kg/mol, $M_w$ = 13 kg/mol, PDI = 1.65. $^1$H NMR (500 MHz, $CDCl_3$): $\delta$ 0.56−0.90 (br, 26H), 1.57 (br, 4H), 1.96−2.08 (br, 4H), 7.20 (br, 2H), 7.83 (br, 1H), 7.56−7.67 (br, 6H), 7.88 (br, 1H), 8.13 (br, 1H), 8.60 (br, 1H). Anal. Calcd for $C_{39}H_{46}N_2S$: C, 81.48; H, 8.07; N, 4.87; S, 5.58. Found: C, 78.06; H, 7.90; N, 3.82; S, 4.59.

*Poly*[*2,6-*(*4,4-bis*(*2-ethylhexyl*)*-4H-cyclopenta*[*2,1-b:3,4-b′*]*-dithiopheneylenevinylene*)*-alt-4,7-*(*2,1,3-benzothiadiazole*)] (***PCPDTVBT**, **P4***). The polymer was synthesized following the same procedure as **P1** with the respective monomers. Yield = 72%. GPC: $M_n$ = 7.6 kg/mol, $M_w$ = 15 kg/mol, PDI = 1.97. $^1$H NMR (500 MHz, $CDCl_3$): $\delta$ 0.66−1.03 (br, 26H), 1.63 (br, 4H), 1.88 (br, 4H), 6.87 (br, 1H), 6.98 (br, 1H), 7.09 (br, 1H), 7.35 (br, 1H), 7.55 (br, 1H), 7.82 (br, 1H), 8.27 (br, 1H), 8.55 (br, 1H). Anal. Calcd for $C_{35}H_{42}N_2S_3$: C, 71.62; H, 7.21; N, 4.77; S, 16.39. Found: C, 68.12; H, 6.61; N, 4.40; S, 15.05.

**Fabrication and Characterization of Polymer Solar Cells.** Polymers **P**−**P4** were codissolved with $PC_{61}BM$ or $PC_{71}BM$ in ODCB with weight ratios of 1:1 or 1:4, respectively. Glass substrates coated with indium tin oxide (ITO) were used as device substrates. The substrates were cleaned in detergent, water, acetone, and isopropyl alcohol under ultrasonication for 15 min each and dried under nitrogen ($N_2$). The substrates were subsequently treated with ultraviolet ozone for 15 min. A thin layer (∼30 nm) of PEDOT:PSS with a resistivity of 1 kΩ·cm was spin-coated onto the substrates. After the substrates were baked at 150 °C for 20 min, the polymer:$PC_{61}BM$/$PC_{71}BM$ blends were spun at 400 rpm for 10 s and at 800 rpm for 60 s on the ITO/PEDOT:PSS substrates inside the glovebox. The samples were left in a covered Petri dish in the glovebox at room temperature overnight. Aluminum electrodes with 100 nm thicknesses were deposited by thermal evaporation at pressures of $2 \times 10^{-6}$ Torr. After electrode deposition, $I-V$ characteristics were recorded in dark and under simulated 1 sun AM 1.5 radiation with a Keithley 2400 source meter. Illumination was achieved with a 91160 300 W Oriel solar simulator equipped with a 6258 ozone-free Xe lamp and an air mass AM 1.5 G filter.

**Computational Methodology.** Analyses of the ground-state structures for **BTZ**, **CPDT**, **FL**, and alternating oligomers of **P1**−**P4** ($n$ = 1−4) were carried out using density functional theory (DFT). The B3LYP functional[17] was used in conjunction with the 6-31G(d,p) basis set. All alkyl chains along the conjugated backbone were truncated to methyl groups to ease the computational cost. Time-dependent DFT (TDDFT) calculations were performed to assess the excited-state vertical transition energies. Absorption spectra were simulated through convolution of the vertical transition energies and oscillator strengths with Gaussian functions characterized by a full width at half-maximum (fwhm) of 0.5 eV. All calculations were performed with Gaussian 03 (Revision E.01),[18] and molecular orbital density plots were generated with ArgusLab 4.0.1.[19]

## Results and Discussion

**Synthesis.** Synthetic routes for the vinylene-linked copolymers (**P**-**P4**) are shown in Scheme 1. Alternating copolymer **P** was synthesized via a Suzuki polycondensation reaction, where **BTZ** was used as the electron acceptor unit and **FL** was the electron donor unit. Alkyl thiophene units were used to improve the solubility of the copolymers. The Suzuki coupling between 2,7-bis(4′,4′,5′,5′,-tetramethyl-2′-vinyl-1′,3′,2′-dioxaborate)-9,9-bis(2-dedecyl)fluorene (**1**) and dibromo compound **2** yielded polymer **P** with a number-averaged molecular weight ($M_n$) of 22 kg/mol and polydispersity index (PDI) of 3.7 as determined by gel permeation chromatography (GPC) (Table 1). Unlike the alternating copolymer **P**, the random copolymer of **P1** was synthesized by a Stille polycondensation reaction between 9,9-didodecyl-2,7-dibromofluorene (**3**), dibromo compound **2,** and *trans*-1,2-bis(tributylstannyl)ethylene (**4**). The ratio of m:n in **P1** was modulated by controlling the monomer ratio (1:1). The *m*:*n* ratio was determined to be 1:1 by the integral areas of $-CH_2-$ peaks of alkyl groups at fluorene (**FL**) and thiophene units in the polymers, which appear at 2.01 and 2.68 ppm, respectively, in the $^1$H NMR spectra (Figure S1). **P1** had a slightly larger number-averaged molecular weight and degree of polymerization ($M_n$ = 25 kg/mol, $DP_n$ = 21) than **P** ($M_n$ = 22 kg/mol, $DP_n$ = 18). During the molecular weight optimization process, higher molecular weight polymers were achieved from the random polymerization, which was probably due to the use of higher-purity starting materials; we therefore followed the random polymerization procedure for the remaining polymers (**P2** - **P4**). Copolymer **P2** was also synthesized by a Stille reaction using 2,6-dibromo-4,4-bis-(2-ethylhexyl)-4*H*-cyclopenta[2,1-*b*:3,4-*b*′]dithiophene (**5**) to give a smaller band gap (1.79 eV) compared to polymer **P1** (2.08 eV) incorporating **FL**.

**Scheme 1. Synthesis of the Vinylene-Incorporated Copolymers *alternating*-PFVTBT (P), *random*-PFVTBT (P1), PCTVTBT (P2), PFVBT (P3), and PCTVBT (P4)**

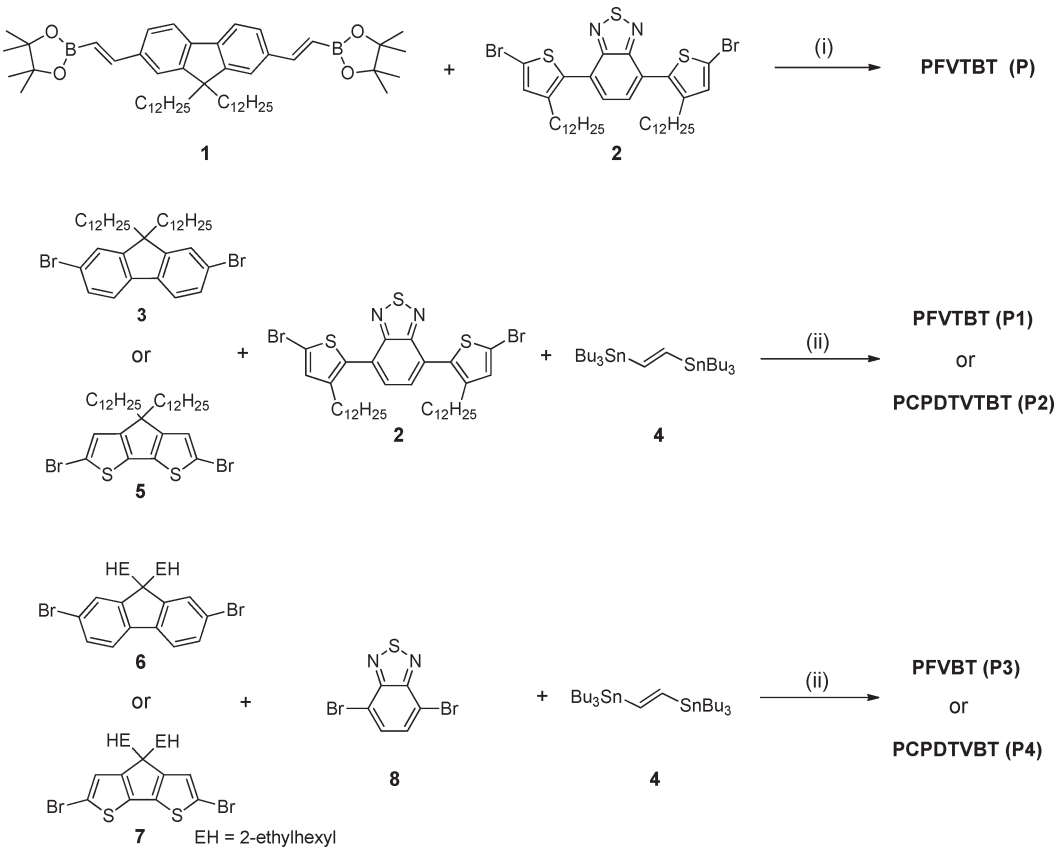


[a] Reagents and condition: (i) $Pd(PPh_3)_4$, 2 M aqueous $K_2CO_3$, Aliquat336, toluene, 90−95 °C, 3 days; (ii) $Pd_2(dba)_3$, tris(*o*-tolyl)phosphine, chlorobenzene, 95−100 °C, 3 days.

**Table 1. Molecular Weights and Optical and Electrochemical Properties of Polymers P−P4**

| polymer | $M_n$ (kg/mol)[a] | PDI[a] | $DP_n$[b] | $HOMO^{ox}$ (eV)[c,d] | $LUMO^{red}$ (eV)[c,d] | $E_g^{elec}$ (eV)[c] |
|---|---|---|---|---|---|---|
| **P** | 22 | 3.67 | 18 | −5.13 | −2.98 | 2.15 |
| **P1** | 25 | 1.60 | 21 | −5.06 | −2.98 | 2.08 |
| **P2** | 13 | 1.68 | 11 | −4.83 | −3.04 | 1.79 |
| **P3** | 8.1 | 1.65 | 14 | −5.15 | −3.20 | 1.95 |
| **P4** | 7.6 | 1.97 | 13 | −4.91 | −3.27 | 1.64 |

[a] Determined from GPC using THF as an eluent and polystyrenes as the standards. [b] Degree of polymerization ($DP_n$) = $M_n$ of polymer/molecular weight of repeating unit. [c] Measured from cyclic voltammetry in ODCB and calibrated based on the oxidation potential of the $Fc/Fc^+$ redox couple. [d] $-HOMO^{ox} \equiv IP^{ox}$; $-LUMO^{red} \equiv EA^{red}$.

4,7-Dibromo-2,1,3-benzothiadiazole (**8**) and *trans*-vinyltin (**4**) were copolymerized with dibromofluorene (**6**) or dibromocyclopnetadithiophene (**7**) to synthesize random compolymers **P3** and **P4**, respectively. These polymers were intentionally synthesized without the adjacent alkylated thiophenes to see if the absorption coefficient would be improved as previously reported for the **TP**-based **ACT-FL** polymer.[7a] In order to improve the solubility of these copolymers, branched alkyl chains (i.e., 2-ethylhexyl groups) were used instead of the linear dodecyl alkyl chains on the donor units. While the polymers **P1** and **P2** containing dodecyl thiophene had $M_n$ of 25 kg/mol and 13 kg/mol, respectively, the molecular weight of copolymers **P3** and **P4** were relatively low ($M_n$ = 8.1 and 7.6 kg/mol, respectively) (Table 1). The low molecular weights of **P3** and **P4** were indeed due to their low solubility. Processing of these polymers was difficult from solution. Thus, improving the molecular weights of **P3** and **P4** will yield polymers with even lower solubility.

In all cases, the polymers were precipitated from the reaction mixtures into methanol. The precipitate was filtered and redissolved in chloroform with palladium scavenger to remove any residual palladium catalyst.[16] Reprecipitation in methanol followed by a washing of the final products with methanol, acetone, and hexane in a Soxhlet apparatus yielded 58−79% for **P**−**P4**. The polymers were soluble in tetrahydrofuran (THF), chloroform, chlorobenzene, and ODCB. The thermal characteristics of **P**−**P4** were determined by thermogravimetric analysis (TGA) and differential scanning calorimetry (DSC). The polymers showed good thermal stability with 5% weight loss temperature ($T_d$) between 316 and 358 °C under nitrogen: 358, 349, 345, 330, and 316 °C for **P**, **P1**, **P2**, **P3**, and **P4**, respectively (Figure S2). The lack of a thermal transition signal in the DSC measurements in the temperature range of 30 - 300 °C indicates that the five polymers are amorphous. This amorphous nature was confirmed by grazing-incidence X-ray scattering (GIXS) studies, which showed no diffraction pattern for both annealed and unannealed films.

**Oligomer Geometric Structure Calculations.** To gain insight into the polymer structure−property relationships,

ground-state geometry optimizations of **FL**, **CPDT**, **BTZ**, **BTZ**-bis(thiophene) (**BTZ-bt**), and oligomers ($n$ = 1−4) of **P1**−**P4** were carried out using density functional theory at the B3LYP/6-31G(d,p) level; select bond lengths for **FL**, **CPDT**, **BTZ**, **BTZ-bt**, and the **P1**−**P4** monomers are detailed in the Supporting Information (Table S1). Alternating (versus random) donor−acceptor oligomer structures were used to ease the computational analysis (*vide infra*). As the individual components were assembled to build the larger oligomer structures, slight changes in bond length versus the isolated structures were observed. In particular, there was generally some decrease of the native bond-length alternation of the individual structures; an exception to this was the **FL** subunit, which underwent stronger bond-length alternation on insertion into the polymer. The influence of heterocycle orientation − as the components comprising the conjugated backbone can be envisioned to take an approximate 0°(*syn*-conformation) or 180° (*anti*-conformation) orientation with respect to each other − was detailed as a check for the component pair **BTZ-bt**. The preferred orientation is the 180° conformation, with the energetic stabilization vs the 0° conformation being on the order of 0.1 kcal/mol. Virtually no difference in bond length is observed for the two orientations; however, the total dipole moment was considerably reduced for the 180° orientation (0.31 D) versus the 0° orientation (2.66 D). The alkyl substitution on the thiophene subunits results in a considerable twist of approximately 45−47° between the thiophene and **BTZ** units in the oligomers.

**Electrochemical Properties and Electronic Structure.** Oxidation and reduction potentials for **P**−**P4** in ODCB were obtained using cyclic voltammetry (CV), as summarized in Table 1. The electrochemical HOMO−LUMO energy gap was determined as the difference between the onsets of the oxidation and reduction potentials ($E_g^{elec} = E_{ox}^{onset} - E_{red}^{onset}$). Ionization potential ($IP^{ox} \approx -HOMO^{ox}$, assuming that Koopmans' theorem holds)[20] and electron affinity ($EA^{red} \approx -LUMO^{red}$) energies were estimated from the onset potential for oxidation and reduction, respectively, and calibrated against the oxidation potential of $Fc/Fc^+$ (4.8 eV below the vacuum level). The $HOMO^{ox}-LUMO^{red}$ gap of **P1** ($E_g^{elec}$ = 2.08 eV) is lower than the gap of **P** ($E_g^{elec}$ = 2.15 eV), and reflects the extended conjugation length of polymer **P1** ($DP_n$ = 18 and 21 for **P** and **P1**, respectively). The $HOMO^{ox}$ levels of **P2** and **P4** containing the **CPDT** unit (−4.83 eV and −4.91 eV, respectively) are higher than those of **P1** and **P3** (−5.06 eV and −5.15 eV, respectively) with the **FL** donor unit, indicative of the stronger electron-donating ability of **CPDT** (Figure 2). Interestingly, both the $HOMO^{ox}$ and $LUMO^{red}$ energy levels of **P3** and **P4**, which lack thiophene groups, are lower (~0.1 eV in $HOMO^{ox}$ and ~0.2 eV in $LUMO^{red}$) compared to their respective **P1** and **P2** counterparts. The degree of lowering the $LUMO^{red}$ energy levels is larger (~0.2 eV) than that of lowering the $HOMO^{ox}$ energy levels (~0.1 eV) between **P1**/**P3** and **P2**/**P4**, resulting in lower band gaps in **P3** and **P4** ($E_g^{elec}$ = 1.95 and 1.64 eV, respectively). The deeper energeric stabilization of the $LUMO^{red}$ energies of **P3** and **P4** can be attributed to the more planar structure, thus allowing for stronger coupling between neighboring **BTZ** units (*vide infra*).

To better understand the evolution of the oxidation and reduction potentials, the electronic structures of the alternating polymer series (as isolated oligomers) were evaluated using DFT at the B3LYP/6-31G(d,p) level of theory; the HOMO and LUMO energies and HOMO−LUMO energy gaps ($E_g$) are given in Table 2; pictorial representations of the frontier molecular orbitals of **FL**, **CPDT**, **BTZ**, **BTZ-bt**, and the **P1**−**P4** monomers are shown in Figure 3. The individual **FL**, **CPDT**, and **BTZ** units have relatively large $E_g$'s (~4 eV), with the HOMO and LUMO energies of **BTZ** being lower, as expected. On substitution with bis(thiophene), the HOMO of **BTZ** destabilizes by 1 eV, while the LUMO stabilizes by 0.13 eV. Thus, the interaction between **BTZ** and the thiophene substituents reduces $E_g$ considerably (down to 3.13 eV). Comparison of the HOMO and LUMO energies of the **P1**−**P4** monomers indicates that the addition of thiophene units to the polymer backbone in **P1** and **P2** slightly destabilizes the HOMO energies (~0.2 eV), while the LUMO energies remain virtually unchanged compared to their counterparts **P3** and **P4**. The pictorial representations of the molecular orbital densities in Figure 3 show that while the HOMO is completely delocalized across the **FL**/**CPDT** and **BTZ** units in **P3** and **P4**, the sizable twist between the thiophene units and the **BTZ** prevents full delocalization in **P1** and **P2**; the thiophene unit adjacent to the **FL**/**CPDT** units possesses considerable HOMO electron density. The LUMO in each monomer is principally localized on **BTZ**, hence the minimal impact of the donor substituent on the LUMO energies in the series.

As the oligomer length is increased to the dimer, $E_g$ reduces by ~0.2−0.5 eV and decreases further (though at a

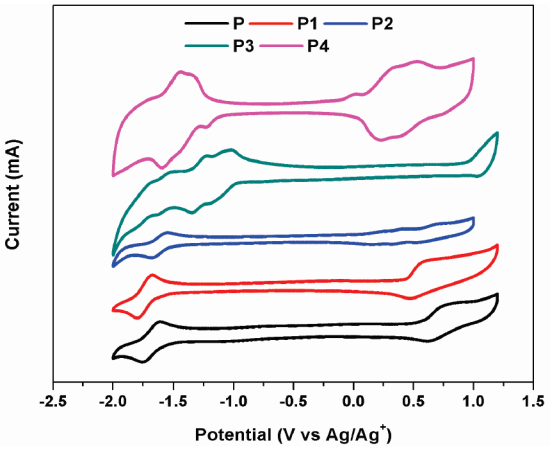


**Figure 2.** Cyclic voltammetry of polymers **P**−**P4** in 0.05 M $TBAPF_6$ in ODCB.

**Table 2. Frontier Molecular Orbital Energies and HOMO−LUMO Energy Gaps ($E_g$) As Determined at the B3LYP/6-31G(d,p) Level of Theory**

| | $n$ | HOMO-1 (eV) | HOMO (eV) | LUMO (eV) | LUMO+1 (eV) | $E_g$ (eV) |
|---|---|---|---|---|---|---|
| **FL** | | | −5.74 | −0.76 | | 4.98 |
| **CPDT** | | | −5.19 | −1.02 | | 4.17 |
| **BTZ** | | | −6.62 | −2.35 | | 4.27 |
| **BTZ-bt** | | | −5.61 | −2.48 | | 3.13 |
| **P1** | 1 | −5.56 | −5.02 | −2.55 | −1.64 | 2.47 |
| | 2 | −5.07 | −4.86 | −2.58 | −2.54 | 2.28 |
| | 3 | −4.92 | −4.83 | −2.59 | −2.56 | 2.24 |
| | 4 | −4.87 | −4.81 | −2.60 | −2.58 | 2.21 |
| **P2** | 1 | −5.47 | −4.75 | −2.53 | −1.8 | 2.22 |
| | 2 | −4.78 | −4.55 | −2.60 | −2.53 | 1.95 |
| | 3 | −4.62 | −4.52 | −2.63 | −2.57 | 1.89 |
| | 4 | −4.57 | −4.51 | −2.65 | −2.60 | 1.86 |
| **P3** | 1 | −6.14 | −5.19 | −2.54 | −1.34 | 2.65 |
| | 2 | −5.33 | −4.91 | −2.66 | −2.51 | 2.25 |
| | 3 | −5.07 | −4.84 | −2.71 | −2.58 | 2.13 |
| | 4 | −4.95 | −4.80 | −2.73 | −2.64 | 2.07 |
| **P4** | 1 | −5.98 | −4.89 | −2.55 | −1.56 | 2.34 |
| | 2 | −5.07 | −4.56 | −2.76 | −2.49 | 1.80 |
| | 3 | −4.77 | −4.46 | −2.85 | −2.63 | 1.61 |
| | 4 | −4.62 | −4.42 | −2.89 | −2.73 | 1.53 |

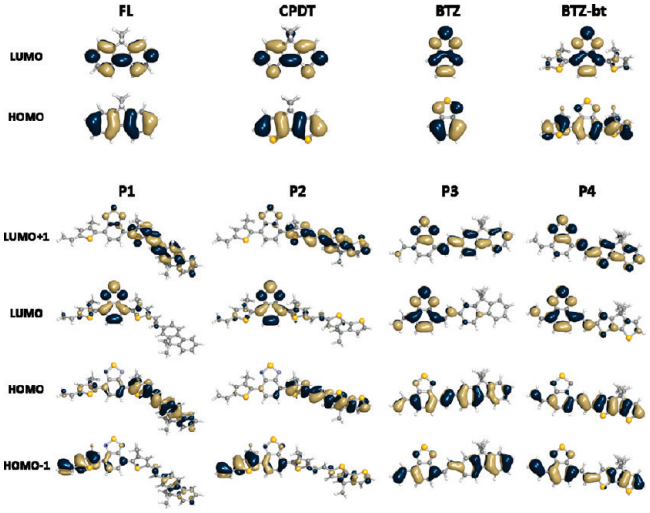


**Figure 3.** Pictorial representations of the frontier molecular orbitals for **FL**, **CPDT**, **BTZ**, **BTZ-bt**, and **P1**−**P4** monomers.

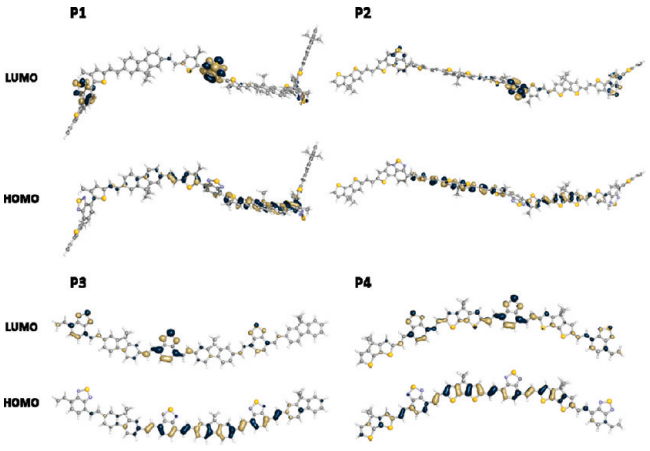


**Figure 4.** HOMO and LUMO wave functions of the (a) **P/P1**, (b) **P2**, (c) **P3**, and (d) **P4** trimer model systems calculated at the B3LYP/6-31G(d,p) level of theory.

slower pace) in the trimer and tetramer. Pictorial representations of the HOMO and LUMO wave functions of the **P1**−**P4** trimers are shown in Figure 4 (Figure S4 for dimer and tetramer). In **P1** and **P2**, the HOMO is principally localized on units consisting of thiophene−vinyl−**FL/CPDT**−vinyl−thiophene. The large twist along the polymer backbones prevents further conjugation across the $\pi$-system. In **P3** and **P4**, the higher degree of coplanarity due to the absence of the alkylated thiophenes allows the HOMO to be conjugated through the **BTZ** units. While the LUMOs are principally localized on the **BTZ**, the more planar backbone in **P3** and **P4** allows for stronger coupling between neighboring **BTZ** units, resulting in a slight energetic stabilization of the LUMO energies. The trend in $E_g$ for the oligomer series follows **P1** > **P3** > **P2** > **P4**, which corresponds well with the experimental data (Table 1). These results indicate that addition of the alkylated thiophene units increases $E_g$ (**P1** > **P3** and **P2** > **P4**), while **CPDT** provides a significant reduction in $E_g$ (**P1** > **P2** and **P3** > **P4**) versus **FL**.

**Optical Properties.** The optical properties of **P**−**P4** were investigated in solution (ODCB) and in thin films, Table 3. For the alternating polymer **P** and the random polymer **P1**, the normalized absorption spectra in ODCB and absorption coefficient in the thin films are shown in Figure 5. The absorption of **P1** was red-shifted in both solution ($E_g^{opt}$ = 2.07 eV) and thin film ($E_g^{opt}$ = 2.01 eV) versus **P** ($E_g^{opt}$ = 2.15 eV in solution and 2.13 eV in thin film). It is worth noting that the absorption coefficient of **P1** is 1.2 × $10^5$ $cm^{-1}$, ~1.3× larger than that of **P** at all wavelengths. The stronger absorption is attributed to the higher molecular weight and degree of polymerization of **P1**, which can influence intermolecular packing. The fact that the solid-state spectrum ($\lambda_{onset}$ = 617 nm) of **P1** is more red-shifted than the solution spectrum ($\lambda_{onset}$ = 600 nm) suggests that the **P1** polymer backbone has more ordered interchain packing compared to **P** ($\lambda_{onset}$ = 576 nm in solution and 581 nm in thin film).[21] In comparison to **PF-DBT** and **PP-DBT** (which contain phenyl groups, $E_g^{opt}$ = 2.32 and 2.24 eV, respectively), the absorption spectra of **P** and **P1** were red-shifted (28 - 83 nm in thin films, $E_g^{opt}$ = 2.13 and 2.01 eV, respectively) due to being less sterically hindered structures. Further, **P** and **P1** showed larger absorption coefficients (9.2 × $10^5$ and 1.2 × $10^5$ $cm^{-1}$, respectively) than **PF-DBT** and **PP-DBT** (5.2 × $10^4$ and 6.8 × $10^4$ $cm^{-1}$, respectively). Although both **P** and **P1** show broad absorption in the region of 300−650 nm and lower band gaps compared to **PF-DBT** and **PP-DBT**, the $\lambda_{max}$ values (479 and 500 nm for **P** and **P1**, respectively) are still small compared to $\lambda_{max}$ (545 nm) of the poly[2,7-(9-(2′-ethylhexyl)-9-hexylfluorene)-*alt*-5,5-(4′,7′-di-2-thienyl-2′,1′,3′-benzothiadiazole)] (**PFDTBT**) in the thin film.[22] The reduced $\lambda_{max}$ vs **PFDTBT** is related to the twisted (~45°) polymer backbone caused by the steric hindrance of the dodecyl substituents in the vicinity of the **BTZ**-thiophene linkages, which affects the planarity of the polymer backbone and reduces the conjugation length (*vide supra*).[23]

**Table 3. Optical Properties of Polymers P−P4**

| | solution[a] | | | thin films | | |
|---|---|---|---|---|---|---|
| polymer | $\lambda_{max}$ (nm) | $\lambda_{onset}$ (nm) | $E_g^{opt}$ (eV)[b] | $\lambda_{max}$ (nm) | $\lambda_{onset}$ (nm) | $E_g^{opt}$ (eV)[b] |
| **P** | 478 | 576 | 2.15 | 479 | 581 | 2.13 |
| **P1** | 502 | 600 | 2.07 | 500 | 617 | 2.01 |
| **P2** | 568 | 698 | 1.78 | 569 | 714 | 1.74 |
| **P3** | 540 | 633 | 1.96 | 533 | 659 | 1.88 |
| **P4** | 637 | 761 | 1.63 | 637 | 791 | 1.57 |

[a] Measured from UV−vis absorption in ODCB solution. [b] Estimated from the onset of the absorption spectra.

The absorption spectra of the random polymers **P1**-**P4** are shown in Figure 6. The polymers **P2** and **P4** incorporating **CPDT** units have red-shifted absorptions compared to analogous copolymer containing **FL** units (**P1** and **P3**) in both solution and thin-film. The longer wavelength peaks of polymers **P3** and **P4**, which lack adjacent alkyl thiophenes around the **BTZ** units, are red-shifted compared to **P1** and **P2**, respectively. Thus, the optical band gaps of **P3** and **P4** (1.88 and 1.57 eV, respectively) are smaller than **P1** and **P2** (2.01 and 1.74 eV, respectively) (Table 2). In addition, polymers **P3** and **P4** show larger absorption coefficients (8.3 × $10^4$ $cm^{-1}$ and 1.3 × $10^5$ $cm^{-1}$, respectively) at longer wavelength in thin films (Figure 6b), compared to the absorption coefficients of the **P1** and **P2** (6.9 × $10^4$ $cm^{-1}$ and 9.0 × $10^4$ $cm^{-1}$, respectively). The larger absorption coefficients for the primary absorptions are attributed to the enhanced HOMO−LUMO overlap, resulting from a more delocalized molecular orbital density for both HOMO and LUMO wave functions of **P3** and **P4**, irrespective of their lower molecular weights (*vide supra*).[7a] We additionally note that the energetic differences between $E_g^{elec}$ and $E_g^{opt}$ are small, indicating that these materials may have very small exciton binding energies; further study to better assess this point is required.

Calculated excited-state vertical transition energies, oscillator strengths, and transition electronic configurations as determined with TDDFT at the B3LYP/6-31G(d,p) level of

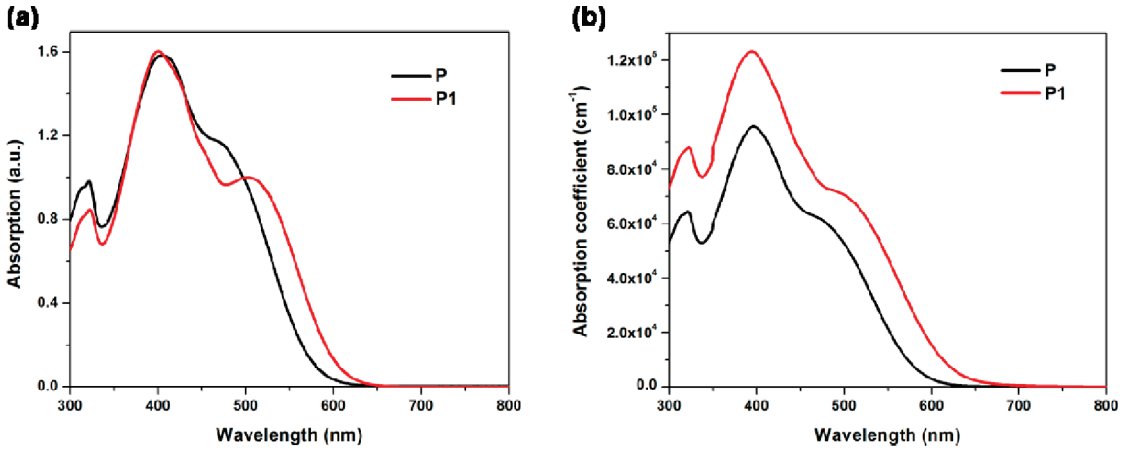


**Figure 5.** Absorption spectra of polymers **P** and **P1** (a) in ODCB and (b) of the thin films. Absorption coefficients of the thin films were obtained using the equation (optical density × ln10)/thickness.

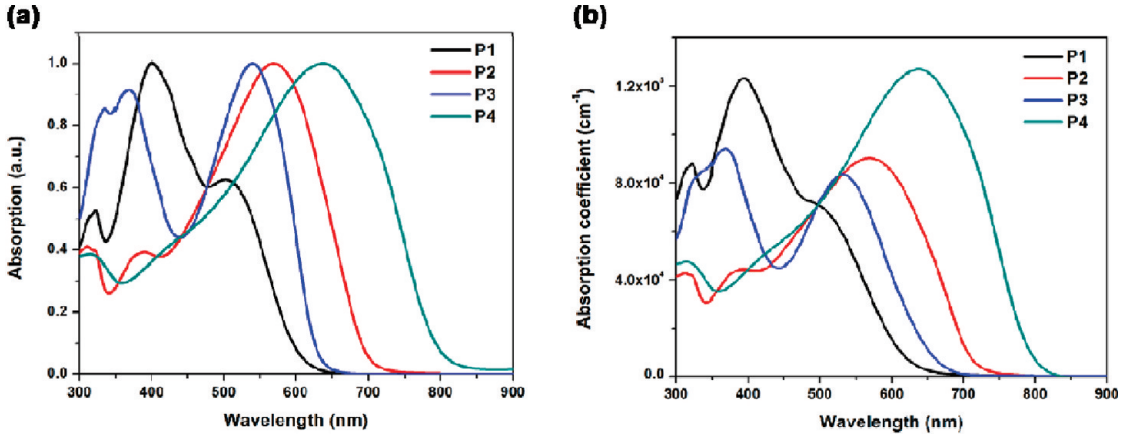


**Figure 6.** Absorption spectra of polymers **P1**−**P4**: (a) in ODCB and (b) of the thin films.

**Table 4. Excited-State Vertical Transition Energies ($E_{vert}$, eV), Oscillator Strengths (Arbitrary Units), and Electronic Configuration of the First Excited State As Determined with TDDFT at the B3LYP/6-31G(d,p) Level of Theory**

| | *n* | $E_{vert}$ (eV) | *f* (au) | configuration |
|---|---|---|---|---|
| **P1** | 1 | 2.09 | 0.46 | HOMO → LUMO [0.67] |
| | 2 | 1.93 | 1.23 | HOMO → LUMO [0.57]; HOMO → LUMO+1 [0.31]; HOMO-1 → LUMO+1 [0.20] |
| | 3 | 1.88 | 1.65 | HOMO → LUMO [0.57]; HOMO → LUMO+1 [0.23]; HOMO-1 → LUMO+1 [0.16]; HOMO-1 → LUMO+2 [0.15]; HOMO-2 → LUMO+2 [0.12] |
| | 4 | 1.86 | 2.15 | HOMO → LUMO [0.53]; HOMO → LUMO+1 [0.21]; HOMO-1 → LUMO [0.12]; HOMO-1 → LUMO+1 [0.23]; HOMO-1 → LUMO+2 [0.16]; HOMO-2 → LUMO+3 [0.11] |
| **P2** | 1 | 1.89 | 0.48 | HOMO → LUMO [0.67] |
| | 2 | 1.66 | 1.92 | HOMO → LUMO [0.65]; HOMO → LUMO+1 [0.12]; HOMO-1 → LUMO+1 [0.13] |
| | 3 | 1.58 | 3.13 | HOMO → LUMO [0.63]; HOMO-1 → LUMO+1 [0.19] |
| | 4 | 1.55 | 4.33 | HOMO → LUMO [0.59]; HOMO → LUMO+1 [0.11]; HOMO-1 → LUMO+1 [0.26]; HOMO-2 → LUMO+2 [0.11] |
| **P3** | 1 | 2.34 | 0.51 | HOMO → LUMO [0.64]; HOMO → LUMO+1 [0.12] |
| | 2 | 1.97 | 1.88 | HOMO → LUMO [0.64] |
| | 3 | 1.84 | 3.10 | HOMO → LUMO [0.64]; HOMO → LUMO+1 [0.13]; HOMO-1 → LUMO [0.12] |
| | 4 | 1.78 | 4.21 | HOMO → LUMO [0.61]; HOMO → LUMO+1 [0.17]; HOMO-1 → LUMO [0.12]; HOMO-1 → LUMO+1 [0.16] |
| **P4** | 1 | 2.13 | 0.63 | HOMO → LUMO [0.62]; HOMO → LUMO+1 [0.16] |
| | 2 | 1.62 | 2.41 | HOMO → LUMO [0.63] |
| | 3 | 1.40 | 3.89 | HOMO → LUMO [0.64]; HOMO-1 → LUMO+1 [0.11] |
| | 4 | 1.30 | 5.03 | HOMO → LUMO [0.64]; HOMO-1 → LUMO+1 [0.15] |

theory are given in Table 4. For the **P1**−**P4** oligomer series, the $S_0 \rightarrow S_1$ transition is primarily a HOMO → LUMO transition (57%−90%), though other close-lying valence molecular orbitals (in particular, HOMO-2, HOMO-1, LUMO+1, and LUMO+2) do contribute to the excitation; this is especially true for the longer oligomeric structures. As with the molecular orbital energies, a significant decrease in vertical transition energy occurs on going from the monomer to dimer structure, with the drop leveling off considerably on extension to the trimer and tetramer. The trend in $E_{vert}$ for the four oligomer series follows **P1** > **P3** > **P2** > **P4**, which is similar to the trends in HOMO−LUMO gaps. A substantial increase in oscillator strength also occurs as the number of repeat units increases through the tetramer.

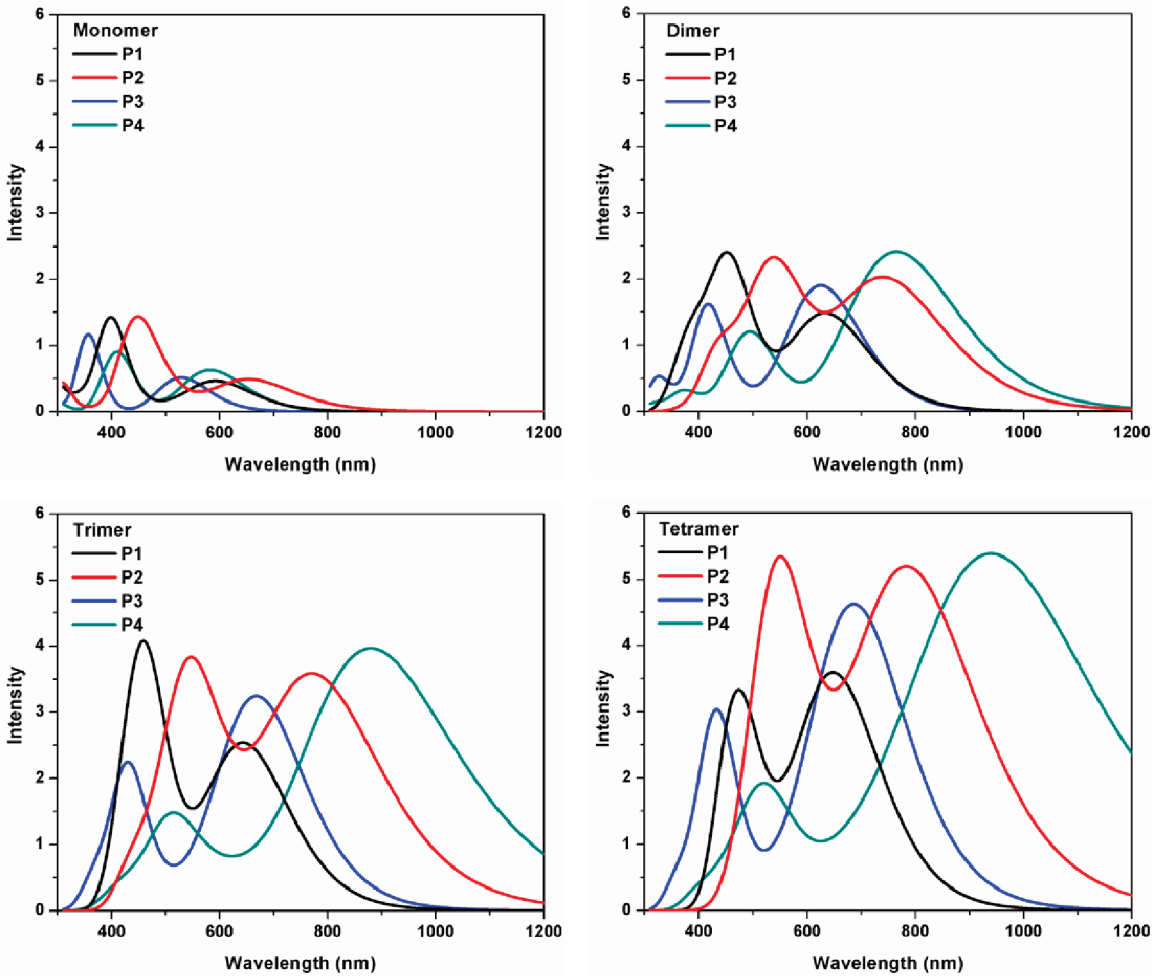


**Figure 7.** Simulated absorption spectra for the alternating oligomer ($n$ = 1−4) constructs of **P1**−**P4** as determined with TDDFT at the B3LYP/6-31G(d,p) level.

Simulated absorption profiles for the monomer, dimer, trimer, and tetramer structures based on the TDDFT vertical transition energies are given in Figure 7, while Figure 8 shows the transition dipole moments as a function of wavelength of the vertical transitions for the oligomers ($n$ = 1−4). The simulated absorption profiles show two prominent − one low energy and one high energy − absorption peaks, in agreement with the empirical spectra. As can be seen from the calculated absorption profiles, the relative maximum peak position for the longest wavelength is not well reproduced for the monomer structure: while the energy of the first excited state from the empirical spectra follows **P1** > **P3** > **P2** > **P4** (Figure 6b), the calculated energy of the **P1** and **P4** monomers are too large with respect to **P3** and **P2**, respectively. This should serve as a note of caution as donor−acceptor polymer optical properties have been previously predicted solely based on quantum chemical analysis of monomeric structures, whose properties are known to deviate substantially from those of longer oligomers.[24] Going to the dimer structure improves the comparison considerably, though the first transitions of **P1** and **P3** are virtually stacked on top of each other. Continuing to the trimer and tetramer structures further improves the correspondence between the theoretical and empirical results (Figure 6b). In particular, the trends of the empirically determined absorption wavelengths appear to be well reproduced as the conjugated path is extended and the oligomer begins to better resemble the polymer. It is expected that the calculated absorption properties will continue to red shift until the effective conjugation length of the polymer is reached.[24,25] Note, however, that the peak positions of the calculated absorption peaks are red-shifted versus the empirical data; this is a known problem with vertical transition energies determined with TDDFT using the B3LYP functional, and is a function of the propensity of B3LYP to favor delocalized solutions due to the self-interaction error in density functional theory.[26,27] We also note the sizable increase in the transition dipole moment of the principal, low energy absorption peak with increasing oligomer size, which is indicative of the larger spatial overlap between the primary $\pi-\pi^*$ orbitals involved in the transitions; it is expected that the continual increase in transition dipole moment will level off at the effective conjugation length of the polymer. In addition, the oligomer structures without the alkylated thiophene units (**P3** and **P4**) possess transitions with the largest transition dipole moments, again showing the importance of an extended conjugated path free from the influence of torsions on the optical properties.

As noted above, Figures 7 and 8 also reveal the presence of a second, higher-energy peak with considerable transition dipole moment, in agreement with the empirical spectra. Analysis of the electronic configurations indicates that the second peak is primarily a $\pi-\pi^*$ transition localized on the donor segments, with the unoccupied $\pi^*$ orbital also having substantial electron density on the thiadiazole fragment of **BTZ**. Again, the transition dipole moment associated with

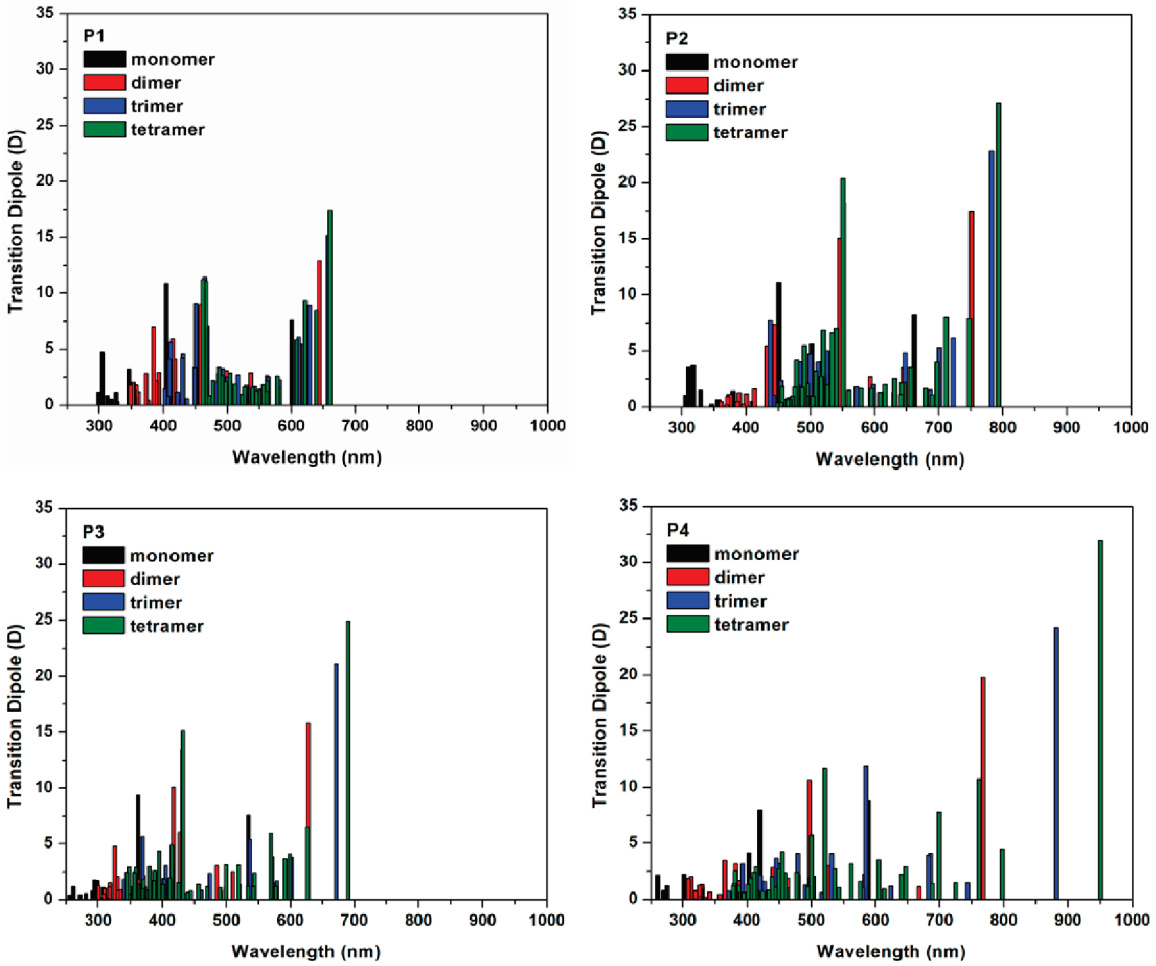


**Figure 8.** Transition dipole moments (D) for the principal excitations for the monomer, dimer, trimer, and tetramer constructs of **P1**−**P4**, calculated with TDDFT at the B3LYP/6-31G(d,p).

the second absorption increases both with oligomer size and planarity of the oligomer backbone.

As noted above, the theoretical analyses of the random polymers **P1**−**P4** were carried out using alternating oligomers, as determining theoretical data for all possible random polymer distributions of the donor−acceptor components would be a difficult task. Indeed, it is difficult to know whether the random polymerization procedure would lead to a polymer with a more regioregular donor−acceptor (D−A) polymer configuration, a more regiorandom D−A polymer configuration, a more block D−A polymer configuration, or some variation thereof. The proportionality of these segment types within the polymer could have an impact on the electronic structure, electrostatics, and optical properties. For the purpose of this work, the calculations were performed to gain insight into the geometric, electronic, and optical properties of the studied polymers. Therefore, realizing the difficulty of the above, calculations on regioregular D−A oligmers were used as a first approximation to describe these properties for the polymer series. Very good correlation between the electronic structure, oxidation and reduction energies, and optical properties (including trends for both the vertical transition energies and transition dipole moments, which correlate to the absorption coefficients) were found for **P1**−**P4**. For example, the empirically determined HOMO−LUMO gaps derived from electrochemical measurements reveal that the transport gaps of **P** (regioregular) and **P1** (regiorandom) differ by 0.07 eV, while the gap differs by 0.3 eV on going from **P1** to **P2** through the use of different donor units. This trend is reproduced well via the density functional theory calculations. In addition to providing information pertaining to the trends, the density functional theory calculations provide valuable insight that could not be gained by experiment alone. For example, the larger computed transition dipole moments for **P2** and **P4** (compared to **P1** and **P3**, respectively) were determined to be a function of larger spatial overlap between the primary $\pi-\pi^*$ orbitals involved in the first vertical transition, which in turn was a function of the greater degree of planarity and greater conjugation path length that evolved with the removal of the alkylated thiophene units from the conjugated backbone. Thus, in spite of the necessary simplifications that were made, the theoretical analyses of the geometric structure, electronic structure, and excited-state vertical transitions presented provide direct insight into the interplay between the structural modifications and resulting electronic and optical changes.

**Hole Mobility.** Hole mobilities for **P**−**P4** were measured using the space charge limited current (SCLC) model[14] with a device structure of ITO/PEDOT:PSS/polymer/Au. Hole mobilities of $1.3 \times 10^{-5}$ cm$^2$/(V s), $1.0 \times 10^{-5}$ cm$^2$/(V s), $1.4 \times 10^{-7}$ cm$^2$/(V s), and $8.5 \times 10^{-6}$ cm$^2$/(V s) were measured for **P1**, **P2**, **P3**, and **P4**, respectively. Even though the mobilities of amorphous polymers **P1**−**P4** are not as high as that of crystalline **P3HTV** ($1.6\times 10^{-3}$ cm$^2$/(V s)),[28] they are comparable with amorphous phenylenevinylene polymers, such as poly[2-methoxy-5-(3′,7′-dimethyloxy)-*p*-phenylenevinylene] (**MDMO-PPV**) ($5 \times 10^{-7}$ cm$^2$/(V s)).[29] It is noteworthy

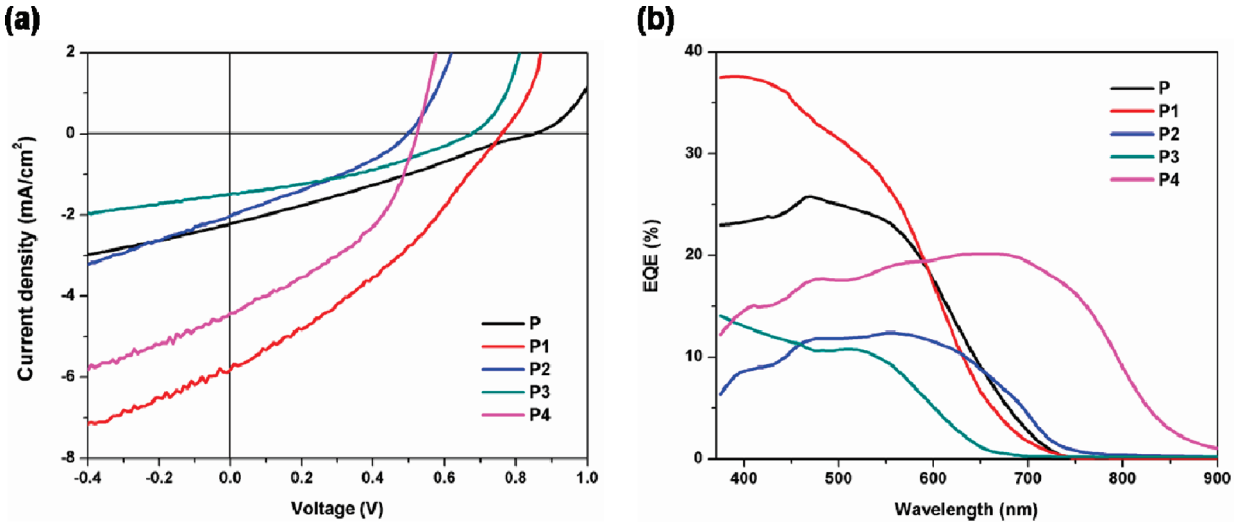


**Figure 9.** (a) $I-V$ curves of P−P4 based solar cell devices under illumination with AM 1.5 G solar simulated light (100 mW/cm$^2$). (b) External quantum efficiency (EQE) of the PSCs.

that **P1** and **P2** have higher mobilities than **P3** and **P4**, though the **P1** and **P2** polymer backbones are more twisted. It is also important to recognize that all of these polymers are amorphous. According to these observations, it seems that the measured SCLC mobilities are scaling with the molecular weights and the length of $\pi$-conjugation units of these amorphous polymers. In comparison to **P1** and **P3**, **P1** has a larger molecular weight and degree of polymerization ($M_n$ = 25 kg/mol, $DP_n$ = 21) than **P3** ($M_n$ = 8.1 kg/mol, $DP_n$ = 14), indicating more extended $\pi$-conjugation units. In the case of **P2** and **P4**, **P2** has a slightly increased conjugated path due to the thiophene groups appended to **BTZ**, although $DP_n$ of **P2** is smaller than **P4**. The effect of molecular weight and degree of polymerization was also observed between the polymers **P** and **P1** ($M_n$ = 22 and 25 kg/mol, $DP_n$ = 18 and 21 for **P** and **P1**, respectively): the diode mobility of **P1** is an order of magnitude larger compared to that of **P** ($\mu_{diode}$ = $1.2 \times 10^{-6}$ cm$^2$/(V s)). This indicates that the charge carrier mobility of amorphous polymers is most likely a function of the molecular weight (the length of $\pi$-conjugation units), which can influence interchain polymer packing, film-forming quality, and intrachain hopping.[4b,11] However, a more detailed study with a same amorphous polymer with different molecular weight will be required to draw any general conclusion. In general, charge carrier mobility depends on many parameters, such as direction of packing or $\pi-\pi$ stacking distance in crystalline or semicrystalline polymers.[7a,30] Interestingly, recently reported polymer hole mobilities (i.e., **P3HT** and bithiazole-based copolymers)[15b,11] that exhibit crystalline patterns in X-ray diffraction also show charge-carrier mobility dependence with molecular weight.

**Photovoltaic Properties.** Bulk heterojunction photovoltaic devices were fabricated with a structure of ITO/PEDOT−PSS/polymer:PCBM/Al, using a polymer:fullerene-derivative blend in a weight ratio of 1:1 or 1:4 w/w, to investigate photovoltaic performance in polymer solar cells (PSC). Figure 9 shows the $I-V$ curves and external quantum efficiency (EQE) for solar cells under simulated 1 sun AM 1.5 G radiation (100 mW/cm$^2$); optimized photovoltaic properties are summarized in Table 5. Random polymer **P1** has a larger short circuit current ($J_{sc}$ = 5.82 mA/cm$^2$) compared to the alternating polymer **P** ($J_{sc}$ = 4.05 mA/cm$^2$). This difference originates from the stronger absorption and larger hole mobility of **P1**, considering the minor differences in open circuit voltage ($V_{oc}$) and fill factor (FF) between

**Table 5. Photovoltaic Properties of Polymer Solar Cells**[a]

| polymers | $\mu_{diode}$ (cm$^2$/(V s))[b] | $V_{oc}$ (V) | $J_{sc}$ (mA/cm$^2$) | FF (%) | PCE (%) |
|---|---|---|---|---|---|
| **P** | $1.2 \times 10^{-6}$ | 0.785 | 4.05 | 0.28 | 0.84 |
| **P1** | $1.3 \times 10^{-5}$ | 0.765 | 5.82 | 0.32 | 1.42[c] |
| **P2** | $1.0 \times 10^{-5}$ | 0.495 | 2.03 | 0.32 | 0.32 |
| **P3** | $1.4 \times 10^{-7}$ | 0.675 | 1.49 | 0.36 | 0.36[c,d] |
| **P4** | $8.5 \times 10^{-6}$ | 0.525 | 4.42 | 0.41 | 0.95 |

[a] Optimum devices were fabricated with polymer:$PC_{71}BM$ (1:4). [b] Devices spin-coated from polymer solution in ODCB. [c] Annealed at 100 °C for 5 min. [d] Using P3:$PC_{61}BM$ (1:1) blend.

**P**- and **P1**-based solar cells. Power conversion efficiencies of 0.84% and 1.42% for **P** and **P1**, respectively, were achieved (Table 5). The blend of polymer **P1**:$PC_{71}BM$ produced a larger EQE, up to 38%, at 375−450 nm compared to **P**:$PC_{71}BM$ based cells (26% at 375−450 nm), indicating more efficient generation of charge carriers in the **P1** device (Figure 9b).

As described above, the reasons behind the higher PCE for random **P1** are stronger absorption (larger absorption coefficient) in the UV−vis region of the solar spectrum and a higher charge (hole) carrier mobility, which were attributed to the higher molecular weight of **P1** compared to **P**. For the photovoltaic performance of polymer solar cells, molecular weight plays a significant role in controlling PCE,[31] in addition to regioregularity.[3d] Since the vinylene polymers are not very rigid, and in this case regioregularity does not promote a great deal of crystallinity; therefore, other factors (e.g., molecular weight) play a greater role. We believe that if the molecular weights of **P2**−**P4** could be improved, a higher PCE should be expected than their alternating polymers. As summarized in Table 1, higher molecular weight polymers (**P1** versus **P**) were achieved from the random polymerization; we therefore followed the random polymerization procedure for the remaining polymers (**P2**−**P4**). Additionally, the molecular weights of **P3** and **P4** were limited by poor solubility.

Comparing PSC's with the random copolymers **P1**−**P4**, the best performance was the 1.42% PCE for the **P1**:$PC_{71}BM$ (1:4 w/w) blend, with $J_{sc}$ of 5.82 mA/cm$^2$, $V_{oc}$ of 0.765 V, and FF of 0.32 (Table 5). The FF is low in the **P1**-based cells even after extensive morphology optimization, and may be due to low diode mobility in the polymer. **P3** has a larger absorption coefficient at longer wavelength compared to **P1**; however, $J_{sc}$ in the **P3** solar cell device was

reduced to 1.49 mA/cm$^2$, resulting in a 0.36% PCE (Figure 9a). This may be attributed to the even lower diode mobility ($\mu_{diode} = 1.4 \times 10^{-7}$ cm$^2$/(V s)) originating from the low molecular weight of **P3** ($M_n = 8.1$ kg/mol). Moreover, the maximum absorption coefficient of **P1** is larger than that of **P3**. Though no transition temperature was observed in the DSC measurements of **P1** and **P3**, thermal annealing of the solar cells helped to enhance device efficiency (in particular through improvements in $V_{oc}$ and current density, see Table S2).[1c] Specifically, the PCE of the **P1** device was enhanced to 1.42% from 1.13% upon annealing of the device at 100 °C for 5 min.

Comparing the solar cell performance of devices based on **CPDT** containing polymers **P2** and **P4**, **P4** showed a larger PCE of 0.95% owing to the larger $J_{sc}$ (4.42 mA/cm$^2$), which is ascribed to stronger light absorption (larger absorption coefficient) in the thin film that leads to the generation of more excitons, as shown in Figure 9a. Although the hole mobility of **P4** is slightly lower than that of **P2** due to a lower molecular weight ($M_n = 7.6$ kg/mol), stronger absorption (1.4 times) compensates the limited hole mobility on $J_{sc}$ in the devices. EQE measurements (Figure 9b) confirm better charge collection in solar cells based on **P4** owing to the red-shifted and stronger absorption. Whereas the **CPDT** polymers, specifically **P4**, absorb light in a broad spectral range (300−800 nm), the low $V_{oc}$ (0.525 V), which results from the higher HOMO energies, severely limits the solar cell performance (PCE = 0.95%).

From this study, it is evident that solar cell performance depends on a careful balance among the molecular weight, absorption coefficient, charge carrier mobility, and HOMO energy level of the polymers. For different D−A monomer ratios (assuming a similar molecular weight distribution), we would expect changes to the electronic and optical properties of the polymers − e.g., in the case of a 1:2 D−A ratio we might be able to decrease optical band gaps, however, the HOMO energy level would be higher and potentially lead to lower $V_{oc}$. Additionally, the absorption coefficient at longer wavelengths could be made lower with increased incorporation of **BTZ-bt** (benzothiadiazole−bis-alkylated thiophene).

The morphology of the polymer:PCBM blend has a considerable impact on the efficiency of bulk heterojunction solar cells. A nanoscale, bicontinuous network of donor and acceptor materials is crucial to increasing the interfacial area and maximizing charge separation.[1c] Atomic force microscope (AFM) height images of the blends **P1**−**P4** and fullerene derivatives are shown in Figure 10. Though there are variations in the solar cell performance of polymer **P1**−**P4**:PCBM films, all blends formed smooth films with small root-mean-square (rms) roughness (0.38, 0.36, 0.40, and 0.58 nm, respectively), which suggests fine phase separations that should maximize the interfacial area. However, AFM only provides the top surface-morphology of the active layers. It has been shown that vertical phase segregation of donor and acceptor can significantly impact solar cell performance, a feature that cannot be easily probed by AFM.[32]

## Summary and Conclusions

Five new vinylene-incorporating donor−acceptor copolymers were successfully synthesized for use in photovoltaic applications. Solar cell performance depends on the interplay between absorption coefficient, hole mobility, and HOMO energy level. Absorption in the random **FL**-based copolymer **P1** was red-shifted by 36 nm and enhanced compared to the alternating copolymer **P** ($\alpha = 9.6 \times 10^4$ cm$^{-1}$ and $1.2 \times 10^5$ cm$^{-1}$ at 395 nm for **P** and **P1**, respectively). The strength of the optical absorption was improved at longer wavelengths by removing the adjacent alkylated thiophene groups around the acceptor core (**BTZ**) in copolymers due to the better HOMO−LUMO overlap. Although copolymer **P3** had a smaller optical band gap and stronger absorption ($E_g^{elec} = 1.95$ eV, $\alpha = 8.3 \times 10^4$ cm$^{-1}$ at 533 nm) compared to **P1** ($E_g^{elec} = 2.08$ eV, $\alpha = 6.9 \times 10^4$ cm$^{-1}$ at 506 nm), **P1** showed larger PCE ($J_{sc} = 5.82$ mA/cm$^2$, $V_{oc} = 0.765$ V, FF = 0.32, PCE = 1.42%) in solar cell devices, most likely due to the larger hole mobility of the polymer ($\mu_{diode} = 1.3 \times 10^{-5}$ cm$^2$/(V s) and $1.4 \times 10^{-7}$ cm$^2$/(V s) for **P1** and **P3**, respectively). The HOMO energy levels of the **FL**-based polymers (**P1** and **P3**) were deeper (*ca.* ~0.2−0.3 eV) compared to those of **CPDT**-based polymers (**P2** and **P4**), leading to a significant increase in $V_{oc}$. As confirmed by quantum-chemical calculations, copolymer **P4**, which lacks alkylated thiophene groups around the **BTZ** core, showed stronger absorption ($\alpha = 1.3 \times 10^{-5}$ cm$^{-1}$ at 637 nm) resulting in the larger short current density ($J_{sc} = 4.42$ mA/cm$^2$) compared to **P2** ($J_{sc} = 2.03$ mA/cm$^2$). However, the low $V_{oc}$ (0.525 V) originating from the high HOMO energy limited the solar cell performance (0.95%) of the device based on **P4**. DFT calculations of the oligomers of **P1**−**P4** provided detailed insight into the interplay between the structural modifications and optoelectronic properties.

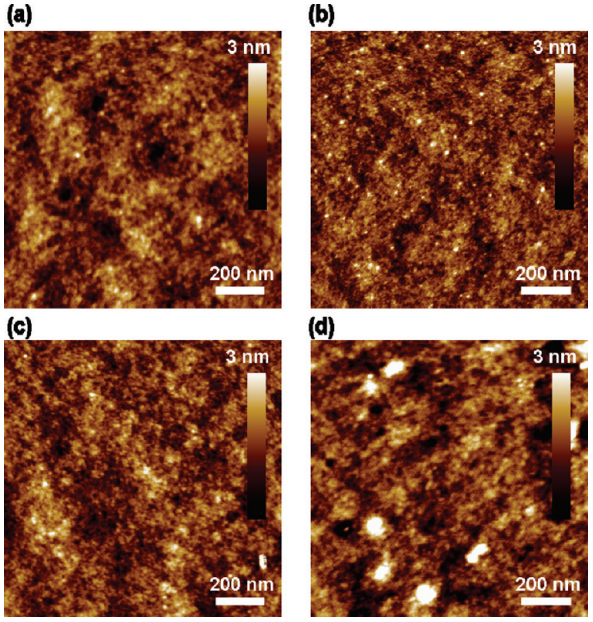


**Figure 10.** AFM height images of (a) **P1**:$PC_{71}BM$ (1:4), (b) **P2**:$PC_{71}BM$ (1:4), (c) **P3**:$PC_{61}BM$ (1:1), and (d) **P4**:$PC_{71}BM$ (1:4) blend.

Solar cell performance depends on the interplay of absorption coefficient, charge mobility, and frontier molecular orbital energy. Even though we were able to improve the absorption coefficient and push the principal absorption to longer wavelengths by removing the alkylated-thiophene units, the low molecular weight of **P3** limited the hole mobility and led to a small $J_{sc}$. Furthermore, **P4** possesses superior absorption properties (large absorption coefficient at long wavelengths) compared to **P2**; however, the higher HOMO energy leads to a low $V_{oc}$ and limits solar cell performance. Nevertheless, the solar cell efficiency for **P1** is among the better performing vinylene incorporated polymers.[8]

**Acknowledgment.** This publication was partially based on work supported by the Center for Advanced Molecular Photovoltaics, Award No KUS-C1-015-21, made by King Abdullah University of Science and Technology (KAUST). We also acknowledge support from the Global Climate and Energy

Program (GCEP) and the Stanford Center for Polymer Interfaces and Macromolecular Assemblies (CPIMA). We thank Prof. Alan Sellinger, Eric Verploegen, Hector A. Becerril, and George Y. Margulis for helpful discussions.

**Supporting Information Available:** Figures showing NMR spectra of polymers, TGA and DSC plots, a table of geometric parameters for **BTZ**, **BTZ-bt**, **CPDT**, **FL**, and **P1**−**P4**, a figure showing pictorial representations of HOMO/LUMO for the dimer and tetramer of **P1**−**P4**, and a table giving optimization of photovoltaic properties. This material is available free of charge via the Internet at http://pubs.acs.org.

## References and Notes


(1) (a) Yu, G.; Gao, J.; Hummelen, J. C.; Wudl, F.; Heeger, A. J. *Science* **1995**, *270*, 1789–1791. (b) Sariciftci, N. S.; Smilowitz, L.; Heeger, A. J.; Wudl, F. *Science* **1992**, *258*, 1474–1476. (c) Thompson, B. C.; Fréchet, J. M. J. *Angew. Chem., Int. Ed.* **2008**, *47*, 58–77. (d) Brabec, C. J.; Sariciftci, N. S.; Hummelen, J. C. *Adv. Funct. Mater.* **2001**, *11*, 15–26. (e) Gunes, S.; Neugebauer, H.; Sariciftci, N. S. *Chem. Rev.* **2007**, *107*, 1324–1338. (f) Ameri, T.; Dennler, G.; Lungenschmied, C.; Brabec, C. J. *Energy Environ. Sci.* **2009**, *2*, 347–363. (g) Krebs, F. C. *Solar Energy Mater. Solar Cells* **2009**, *93*, 394–412. (h) Gonzalez-Valls, I.; Lira-Cantu, M. *Energy Environ. Sci.* **2009**, *2*, 19–34. (i) Kippelen, B.; Brédas, J.-L. *Energy Environ. Sci.* **2009**, *2*, 251–261. (j) Helgesen, M.; Søndergaard, R.; Krebs, F. C. *J. Mater. Chem.* **2010**, *20*, 36–60. (k) Kreb, F. C.; Nielsen, T. D.; Fyenbo, J.; Wadstrøm, M.; Pedersen, M. S. *Energy Environ. Sci.* **2010**, *3*, 512–525.

(2) (a) Kim, J. Y.; Lee, K.; Coates, N. E.; Moses, D.; Nguyen, T.-Q.; Dante, M.; Heeger, A. J. *Science* **2007**, *317*, 222–225. (b) Hoth, C. N.; Choulis, S. A.; Schilinsky, P.; Brabec, C. *J. Adv. Mater.* **2007**, *19*, 3973–3978. (c) Granström, M.; Petritsch, K.; Arias, A. C.; Lux, A.; Andersson, M. R.; Friend, R. H. *Nature* **1998**, *395*, 257–260. (d) Kim, S. -S.; Na, S.-I.; Jo, J.; Tae, G.; Kim, D. -Y. *Adv. Mater.* **2007**, *19*, 4410–4415. (e) Huang, J.; Li, G.; Yang, Y. *Adv. Mater.* **2008**, *20*, 415–419. (f) Krebs, F. C.; Gevorgyan, S. A.; Alstrup, J. *J. Mater. Chem.* **2009**, *19*, 5442–5451. (g) Krebs, F. C.; et al. *Solar Energy Mater. Solar Cells* **2009**, *93*, 1968–1977. (h) Krebs, F. C.; Jørgensen, M.; Norrman, K.; Hagemann, O.; Alstrup, J.; Nielsen, T. D.; Fyenbo, J.; Larsen, K.; Kristensen, J. *Solar Energy Mater. Solar Cells* **2009**, *93*, 422–441.

(3) (a) Li, G.; Shrotriya, V.; Huang, J. S.; Yao, Y.; Moriarty, T.; Emery, K.; Yang, Y. *Nat. Mater.* **2005**, *4*, 864–868. (b) Ma, W. L.; Yang, C. Y.; Gong, X.; Lee, K. H.; Heeger, A. J. *Adv. Funct. Mater.* **2005**, *15*, 1617–1622. (c) Li, G.; Shrotriya, V.; Yao, Y.; Yang, Y. *J. Appl. Phys.* **2005**, *98*, 043704. (d) Kim, Y.; Cook, S.; Tuladhar, S. M.; Choulis, S. A.; Nelson, J.; Durrant, J. R.; Bradley, D. D. C.; Giles, M.; McCulloch, I.; Ha, C.-S.; Ree, M. *Nat. Mater.* **2006**, *5*, 197–203. (e) Ko, C.-J.; Lin, Y.-K.; Chen, F.-C.; Chu, C.-W. *Appl. Phys. Lett.* **2007**, *90*, 063509. (f) Kim, K.; Liu, J.; Namboothiry, M. A. G.; Carroll, D. L. *Appl. Phys. Lett.* **2007**, *90*, 163511.

(4) (a) Blouin, N.; Michaud, A.; Gendron, D.; Wakim, S.; Blair, E.; Neagu-Plesu, R.; Belletete, M.; Durocher, G.; Tao, Y.; Leclerc, M. *J. Am. Chem. Soc.* **2008**, *130*, 732–742. (b) Liang, Y.; Feng, D.; Wu, Y.; Tsai, S.-T.; Li, G.; Ray, C.; Yu, L. *J. Am. Chem. Soc.* **2009**, *131*, 7792–7799. (c) Chen, H.-Y.; Hou, J.; Zhang, S.; Liang, Y.; Yang, G.; Yang, Y.; Yu, L.; Wu, Y.; Li, G. *Nat. Photonics* **2009**, *3*, 649–653. (d) Liang, Y.; Xu, Z.; Xia, J.; Tsai, S.-T.; Wu, Y.; Li, G.; Ray, C.; Yu, L. *Adv. Mater.* **2010**, *22*, E135–E138. (e) Huo, L.; Hou, J.; Chen, H.-Y.; Zhang, S.; Jiang, Y.; Chen, T. L.; Yang, Y. *Macromolecules* **2009**, *42*, 6564–6571. (f) Hou, J.; Park, M.-H.; Zhang, S.; Yao, Y.; Chen, L.-M.; Li, J.-H.; Yang, Y. *Macromolecules* **2008**, *41*, 6012–6018. (g) Yu, C.-Y.; Chen, C.-P.; Chan, S.-H.; Hwang, G.-W.; Ting, C. *Chem. Mater.* **2009**, *21*, 3262–3269.

(5) (a) Blouin, N.; Michaud, A.; Leclerc, M. *Adv. Mater.* **2007**, *19*, 2295–2300. (b) Lee, J. K.; Ma, W. L.; Brabec, C. J.; Yuen, J.; Moon, J. S.; Kim, J. Y.; Lee, K.; Bazan, G. C.; Heeger, A. J. *J. Am. Chem. Soc.* **2008**, *130*, 3619–3623. (c) Peet, J.; Kim, J. Y.; Coates, N. E.; Ma, W. L.; Moses, D.; Heeger, A. J.; Bazan, G. C. *Nat. Mat.* **2007**, *6*, 497–500. (d) Zhu, Z.; Waller, D.; Morana, M.; Gaudiana, R.; Mühlbacher, D.; Scharber, M.; Brabec, C. *Macromolecules* **2007**, *40*, 1981–1086. (e) Mühlbacher, D.; Scharber, M.; Morana, M.; Zhu, Z.; Waller, D.; Gaudiana, R.; Brabec, C. *Adv. Mater.* **2006**, *18*, 2884–2889. (f) Hou, J.; Chen, H.−Y.; Zhang, S.; Li, G.; Yang, Y. *J. Am. Chem. Soc.* **2008**, *130*, 16144–16145. (g) Wong, W.-Y.; Wang, X.-Z.; He, Z.; Djurišić, A. B.; Yip, C.-T.; Cheung, K.-Y.; Wang, H.; Mak, C. S. K.; Chan, W.-K. *Nat. Mat.* **2007**, *6*, 521–527. (h) Park, S. H.; Roy, A.; Beaupre, S.; Cho, S.; Coates, N.; Moon, J. S.; Moses, D.; Leclerc, M.; Lee, K.; Heeger, A. J. *Nat. Photonics* **2009**, *3*, 297–303. (i) Wang, E.; Wang, L.; Lan, L.; Luo, C.; Zhuang, W.; Peng, J.; Cao, Y. *Appl. Phys. Lett.* **2008**, *92*, 033307. (j) Coffin, R. C.; Peet, J.; Rogers, J.; Bazan, G. C. *Nat. Chem.* **2009**, *1*, 657–661.

(6) (a) Mammo, W.; Admassie, S.; Gadisa, A.; Zhang, F.; Inganäs, O.; Andersson, M. R. *Solar Energy Mater. Solar Cells* **2007**, *91*, 1010–1018. (b) Lindgren, L. J.; Zhang, F.; Andersson, M.; Barrau, S.; Hellström, S.; Wendimagegn, M.; Perzon, E.; Inganäs, O.; Andersson, M. R. *Chem. Mater.* **2009**, *21*, 3491–3502. (c) Kitazawa, D.; Watanabe, N.; Yamamoto, S.; Tsukamoto, J. *Appl. Phys. Lett.* **2009**, *95*, 053701.

(7) (a) Mondal, R.; Ko, S.; Norton, J. E.; Miyaki, N.; Becerril, H. A.; Verploegen, E.; Toney, M. F.; Brédas, J.-L.; McGehee, M. D.; Bao, Z. *J. Mater. Chem.* **2009**, *19*, 7195–7197. (b) Becerril, H. A.; Miyaki, N.; Tang, M. L.; Mondal, R.; Sun, Y.-S.; Mayer, A. C.; Parmer, J.; McGehee, M. D.; Bao, Z. *J. Mater. Chem.* **2009**, *19*, 591–593. (c) Zhang, F.; Mammno, W.; Andersson, L. M.; Admassie, S.; Andersson, M. R.; Inganäs, O. *Adv. Mater.* **2006**, *18*, 2169–2173. (d) Ashraf, R. S.; Shahid, M.; Klemm, E.; Al-Ibrahim, M.; Sensfuss, S. *Macromol. Rapid Commun.* **2006**, *27*, 1454–1459. (e) Mondal, R.; Becerril, H. A.; Verploegen, E.; Kim, D.; Norton, J. E.; Ko, S.; Miyaki, N.; Lee, S.; Toney, M. F.; Brédas, J.-L.; McGehee, M. D.; Bao, Z. *J. Mater. Chem.* **2010**, *20*, 5823−5834.

(8) (a) Hou, J.; Tan, Z.; Yan, Y.; He, Y.; Yang, C.; Li, Y. *Macromolecules* **2006**, *39*, 4657–4662. (b) Mei, J.; Heston, N. C.; Vasilyeva, S. V.; Reynolds, J. R. *Macromolecules* **2009**, *42*, 1482–1487. (c) Leclerc, N.; Michaud, A.; Sirois, K.; Morin, J.-F.; Leclerc., M. *Adv. Funct. Mater.* **2006**, *16*, 1694–1704. (d) Wen, S.; Pei, J.; Zhou, Y.; Li, P.; Xue, L.; Li, Y.; Xu, B.; Tian, W. *Macromolecules* **2009**, *42*, 4977–4984.

(9) Wang, Y.; Ma., J.; Jiang, Y. *J. Phys. Chem. A* **2005**, *109*, 7197–7206.

(10) Kroon, R.; Lenes, M.; Hummelen, J. C.; Blom, P. W. M.; Boer, B. D. *Polymer reviews* **2008**, *48*, 531–582.

(11) Li., K.-C.; Huang, J.-H.; Hsu, Y.-C.; Huang, P.-J.; Chu, C.-W.; Lin, J.-T.; Ho, K.-C.; Wei, K.-H.; Lin, H.-C. *Macromolecules* **2009**, *42*, 3681–3693.

(12) Chen, C.-H.; Hsieh, C.-H.; Dubose, M.; Cheng, Y.-J.; Hsu, C.-S. *Macromolecules* **2010**, *43*, 697–708.

(13) Li, Y.; Kim, T.-H.; Zhao, Q.; Kim, E.-K.; Han, S.-H.; Kim, Y.-H.; Jang, J.; Kwon, S.-K. *J. Polym. Sci., A: Polym. Chem.* **2008**, *46*, 5115–5122.

(14) (a) Tsubata, Y.; Suzuki, T.; Miyashi, T. *J. Org. Chem.* **1992**, *57*, 6749–6755. (b) Pilgram, K.; Zupan, M.; Skiles, R. *J. Heterocycl. Chem.* **1970**, *7*, 629–633.

(15) (a) Malliaras, G. G.; Salem, J. R.; Brock, P. J.; Scott, C. *Phys. Rev. B* **1998**, *58*, 13411. (b) Goh, C.; Kline, R. J.; McGehee, M. D.; Kadnikova, E. N.; Frechet, J. M. J. *Appl. Phys. Lett.* **2005**, *86*, 122110.

(16) Nielsen, K. T.; Bechgaard, K.; Krebs, F. C. *Macromolecules* **2005**, *38*, 658–659.

(17) (a) Lee, C. B.; Yang, W.; Parr, R. G. *Phys. Rev. B: Condens. Matter Mater. Phys.* **1988**, *37*, 785–789. (b) Becke, A. D. *Phys. Rev. A: At., Mol., Opt. Phys.* **1988**, *38*, 3098–3100. (c) Becke, A. D. *J. Chem. Phys.* **1993**, *98*, 1372–1377.

(18) Frisch, M. J. et al. *Gaussian03, Revision B.05*; Gaussian, Incorporated: Wallingford, CT, 2004).

(19) Thompson, M. A. *ArgusLab 4.0.1*; Planaria Software LLC: Seattle, WA.

(20) Lu, G.; Usta, H.; Risko, C.; Wang, L.; Facchetti, A.; Ratner, M. A.; Marks, T. J. *J. Am. Chem. Soc.* **2008**, *130*, 7670–7685.

(21) Zen, A.; Pflaum, Z.; Hirschmann, S.; Zhuang, W.; Jaiser, F.; Asawapirom, U.; Rabe, J. R.; Scherf, U.; Neher, D. *Adv. Funct. Mater.* **2004**, *14*, 757–764.

(22) Svensson, M.; Zhang, F.; Veenstra, S. C.; Verhees, W. J. H.; Hummelen, J. C.; Kroon, J. M.; Inganäs, O.; Andersson, M. R. *Adv. Mater.* **2003**, *15*, 988–991.

(23) Jayakannan, M.; Van Hal, P. A.; Janssen, R. A. J. *J. Polym. Sci., A: Polym. Chem.* **2002**, *40*, 251–261.

(24) (a) Meier, H.; Stalmach, U.; Kolshorn, H. *Acta Polym.* **1997**, *48*, 379–384. (b) Rissler, J. *Chem. Phys. Lett.* **2004**, *395*, 92–96. (c) Karsten, B. P.; Viani, L.; Gierschner, J.; Cornil, J.; Janssen, R. A. J. *J. Phys. Chem. A* **2009**, *113*, 10343–10350.

(25) (c) Kuhn, W. *Helv. Chim. Acta* **1948**, *31*, 1780. (a) Meier, H.; Stalmach, U.; Kolshorn, H. *Acta Polym.* **1997**, *48*, 379–384. (b) Gierschner, J.; Cornil, J.; Egelhaaf, H. *J. Adv. Mater.* **2007**, *19*, 173–191.

(26) Reimers, J. R.; Cai, Z. L.; Bilic, A.; Hush, N. S. *Ann. N. Y. Acad. Sci.* **2003**, *1006*, 235.

(27) Gierschner, J.; Cornil, J.; Egelhaaf, H.-J. *Adv. Mater.* **2007**, *19*, 173–191.
(28) Huo, L.; Chen, T. L.; Zhou, Y.; Hou, J.; Chen, H.-Y.; Yang, Y.; Li, Y. *Macromolecules* **2009**, *42*, 4377–4380.
(29) Blom, P. W. M.; de Jong, M. J. M.; Munster, M. G. *Phys. Rev. B* **1997**, *55*, R656–R659.
(30) (a) Kline, R. J.; McGehee, M. D.; Kadnikova, E. N.; Liu, J.; Fréchet, J. M. J.; Toney, M. F. *Macromolecules* **2005**, *38*, 3312–3319. (b) Kline, R. J.; McGehee, M. D.; Kadnikova, E. N.; Liu, J.; Fréchet, J. M. *J. Adv. Mater.* **2003**, *18*, 1519–1522.
(31) Bijleveld, J. C.; Zoombelt, A. P.; Mathijssen, S. G. J.; Wienk, M. M.; Turbiez, M.; de Leeuw, D. M.; Janssen, R. A. J. *J. Am. Chem. Soc.* **2009**, *131*, 16616–16617.
(32) Chen, L.-M.; Hong, Z.; Li, G.; Yang, Y. *Adv. Mater.* **2009**, *21*, 1434–1449.